Journal of Structural Geology 115 (2018) 243–262

Contents lists available at ScienceDirect

Journal of Structural Geology

journal homepage: www.elsevier.com/locate/jsg

Temperature constraints on microfabric patterns in quartzofeldsphatic mylonites, Ribeira belt (SE Brazil)

Carolina Cavalcante[a,*], Leonardo Lagoeiro[a], Haakon Fossen[b,a], Marcos Egydio-Silva[c], Luiz F.G. Morales[d], Filippe Ferreira[e], Thailli Conte[a]

[a] Department of Geology, Universidade Federal do Paraná, Av. Cel. Francisco Heráclito dos Santos, 100, 81531-980, Curitiba, Brazil
[b] Museum of Natural History/Department of Earth Science, University of Bergen, Allégaten 41, N-5007, Bergen, Norway
[c] Instituto de Geociências, Universidade de São Paulo, Rua do Lago, 562, 05508-080, São Paulo, Brazil
[d] Scientific Center for Optical and Electron Microscopy, ETH Zürich, Auguste-Piccard-Hof 1, 8093, Zürich, Switzerland
[e] Bayerisches Geoinstitut (BGI), University of Bayreuth, Universitätsstraße 30, 95447, Bayreuth, Germany

ARTICLE INFO

Keywords:
TitaniQ geothermometry
High-temperature shear zones
Microfabrics
EBSD
Ribeira belt

ABSTRACT

Based on samples from the major high-temperature Três Rios-Além Paraíba-Pádua transpressive shear zone in the Ribeira orogenic belt, Brazil, we discuss the applicability of TitaniQ geothermometry to constrain peak temperature conditions during high-temperature mylonitization of quartzofeldspatic rocks, and explore the microfabrics formed at these conditions. We discuss various aspects of the TitaniQ method and conclude that deformation occurred at temperatures ranging from 612 to 740 ± 20 °C in the studied segment of the shear zone. This high-temperature deformation resulted in relatively large grain size, quartz ribbons and abundant intracrystalline deformation. However, the CPO fabrics are weak, and microstructures suggest that quartz deformation was accommodated by dynamic recrystallization involving grain boundary migration with subsequent grain growth, and later some subgrain rotation during exhumation. We relate the weak fabrics to diffusion processes during or immediately after dynamic recrystallization and dislocation creep, and to the effect of competing slip systems during deformation. In terms of rheology, evidence for Dauphiné twinning in our samples suggest strain softening during mylonitization, and we suggest that such twinning may add to the rheologically weak nature of quartzo-feldspatic portions of hot middle to lower crust.

1. Introduction

Microfabric development exerts strong controls on shear zone evolution, crustal rheology and seismic properties of the middle and lower crust, and depends on a number of factors (e.g., Bürgmann and Dresen, 2008; Lowry and Pérez-Gussinyé, 2011; Almqvist and Mainprice, 2017). Among these, temperature is generally considered to be the most important factor (e.g., Passchier and Trouw, 2005). The relationship between the microstructural evolution of shear zones and temperature has been explored in the laboratory (e.g., Hirth and Tullis, 1992), but the high laboratory strain rates (10^{-5}–10^{-7}) require higher temperatures than those occurring under natural conditions. Therefore, exploring the relationship between microstructural evolution (and consequently material processes responsible for deformation accommodation) and temperature in natural shear zones is essential to meaningfully understand the relationships between microstructural evolution and temperature, and lithospheric deformation in general.

Geothermobarometry can be used to constrain the P-T conditions during deformation if appropriate mineral assemblages are found (e.g. Leloup and Kienast, 1993). However, in many cases, and particularly in quartzofeldspathic rocks, such parageneses are absent, and the determination of temperatures is more difficult. In the last few years the Titanium-in-quartz (TitaniQ) geothermobarometer has become an increasingly common tool to constrain thermal conditions during deformation localization (e.g., Kohn and Northrup, 2009; Ashley et al., 2013; Härtel et al., 2013; Bestmann and Pennacchioni, 2015; Cross et al., 2015). The wide applicability of this geothermobarometer is mainly due to the widespread occurrence of quartz in crustal rocks and the fact that strain often localizes in this phase.

The role of TiO_2 activity at different pressure conditions, the choice of calibration method and the effect of recrystallization mechanisms on the entrapment of Ti in quartz are still rather unclear (e.g., Negrini et al., 2014; Nachlas and Hirth, 2015; Thomas et al., 2015). For example, TitaniQ has successfully been applied to estimate temperature

* Corresponding author.
E-mail addresses: geanecarol@gmail.com, gcarolina.cavalcante@ufpr.br (C. Cavalcante).

https://doi.org/10.1016/j.jsg.2018.07.013
Received 1 March 2018; Received in revised form 18 July 2018; Accepted 19 July 2018
Available online 04 August 2018

conditions during dynamic recrystallization of mylonites deformed at temperatures between ≤400 and ~475 °C (e.g., Kohn and Northrup, 2009; Härtel et al., 2013). However, some studies suggest that pre-existing Ti concentrations are not reset in mylonites recrystallized by subgrain rotation (SGR) and bulging (BGL) at temperatures below 500 °C (e.g., Grujic et al., 2011). Furthermore, under high temperature conditions (> 540 °C), the Ti content in quartz is only completely re-equilibrated (i.e. no inherited Ti remaining) if the dominant recrystallization mechanism is grain boundary migration (GBM; Grujic et al., 2011; Nachlas and Hirth, 2015; Thomas et al., 2015).

The choice of TitaniQ calibration is another subject of discussion (e.g., Nachlas et al., 2014; Thomas et al., 2015). Nachlas et al. (2014), for example, applied the calibrations of Thomas et al. (2010) and Huang and Audétat (2012) to estimate temperatures of undeformed and deformed quartz grains. The results obtained using the calibration of Huang and Audétat (2012) yielded temperatures ~100 °C higher than those obtained from the calibration of Thomas et al. (2010). Huang and Audétat's calibration provided temperatures that were similar to those determined by classical thermobarometry from other metamorphic assemblages. However, temperatures obtained using the Thomas et al. (2010) calibration closely agreed with oxygen isotope thermometry for their studied quartz grains, which is more likely to reflect the conditions of quartz recrystallization.

The recent experiments conducted by Thomas et al. (2015) identified variations in experimental conditions and disequilibrium solubility of Ti in quartz in Huang and Audétat's calibrations. This lead them to conclude that the calibration by Thomas et al. (2010), in which chemical evidence suggest that the experiments reached the equilibrium solubility of Ti in quartz, reliably estimate Ti-in-quartz solubility at *P-T* conditions up to 20 kbar and 1000 °C.

The TitaniQ geothermobarometer has been calibrated under static experimental conditions (Wark and Watson, 2006; Thomas et al., 2015), and only a few studies have investigated the relationship between dynamic recrystallization and titanium uptake or retention in quartz (e.g., Kohn and Northrup, 2009; Grujic et al., 2011; Nachlas et al., 2014). To better understand the role of dynamic recrystallization processes on the Ti content in quartz, we apply the TitaniQ geothermobarometer on quartzofeldsphatic mylonites that crop out along the high-temperature Três Rios - Além Paraíba - Pádua shear zone (SE Brazil). We discuss the temperature estimates obtained from the calibrations of Thomas et al. (2010) and Huang and Audétat (2012), and compare them with previously published classical geothermobarometry estimates from this region. Furthermore, we discuss which calibration gives the most proper temperature estimates for the dynamic recrystallization of quartz. Finally, we view our microstructural observations, accompanied by crystallographic preferred orientation (CPO) measurements through the Electron Backscatter Diffraction (EBSD) technique, in the light of these temperature estimates and briefly discuss the results in terms of rheologic behavior of the lower crust.

2. Geologic setting and temperature estimates along Ribeira Belt

The Ribeira belt is among the youngest elements of the Pan-African-Brasiliano orogenic system, with collisional events occurring from the late Neoproterozoic and into the Paleozoic (Schmitt et al., 2004; Heilbron et al., 2017). It extends for over 1500 km along the SE Brazilian coast from southern Bahia State to Uruguay (Cordani et al., 1973) and was formed by oblique collision between the São Francisco and West Congo cratons during the formation of Western Gondwana, at around 670–480 Ma (Trouw et al., 2000; Bento dos Santos et al., 2007; Schmitt et al., 2016).

In this work, we focus on the Três Rios–Além Paraíba–Pádua shear zone, which is a ~20 km wide and 120 km long dextral shear zone located within the central part of the transpressional Ribeira belt (Fig. 1). The Ribeira belt consists of an anastomosing network of NE-SW to NNE-SSW trending shear zones with associated mylonitic fabrics (Fig. 2). The mylonitic foliation dips 50–90° toward the SE in the study area and carries a subhorizontal stretching lineation. The Além Paraíba–Pádua segment is interpreted as the root of a positive flower structure that resulted from early-stages of the Brasiliano orogenic history (Machado, 1984; Vauchez et al., 1994; Bento dos Santos et al., 2009), and its high-temperature mylonitic rocks and textures, particularly its well-developed ribbon-quartz fabrics, have been discussed in several previous studies (Hippertt et al., 2001; Passchier and Trouw, 2005; Trouw et al., 2010).

The Três Rios–Além Paraíba–Pádua shear zone developed under amphibolite to granulite facies conditions, estimated to 807–877 °C at 600–700 MPa to 734–743 °C at 500 MPa by Porcher et al. (1995), and 661–896 °C at 700 MPa by Bento dos Santos et al. (2010). The peak metamorphism has been dated at 575 ± 20 Ma (Machado et al., 1996; Brueckner et al., 2000).

Pseudosection diagrams for mylonitic rocks from the Além Paraíba-Santo de Pádua shear zone segment suggest that the mylonitization occurred under retrograde conditions (785–615 °C and 820–640 MPa), coeval with the metamorphism of other major rock types, especially charnockites (e.g., Bento dos Santos et al., 2010). Bento dos Santos et al. (2010) suggest that the metamorphic peak recorded in rocks from Santo Antônio de Pádua occurred at 800–900 °C and 800–900 MPa. Further north, Karniol et al. (2009) estimated metamorphic peak temperatures between 680 and 748 °C and pressures between 650 and 700 MPa in mylonitic gneisses from the Italva region, while further south, in the Curitiba Terrain, Faleiros et al. (2016) reported GBM under temperatures > 600–830 °C for quartz from paragneisses from the Turvo Cajati Formation.

3. Samples: description and location

The samples used in this study were collected close to Três Rios (southern), Além Paraíba (central) and Santo Antônio de Pádua (northern part of the shear zone section) regions (Fig. 2). Six samples of mylonitic gneisses (ALP9, ALP16, ALP27a, ALP31, JUNALP4 and JUNALP8) were selected for TitaniQ analyses and crystallographic orientation measurements (Fig. 2). These rocks are characterized by a gneissic banding formed by alternating biotite-hornblende and quartz-feldspar layers and a mylonitic foliation. Rocks from the Três Rios region (Fig. 3a and b) are composed of feldspar (35–70%), quartz (15–50%), hornblende (~15%), biotite (~7%), and orthopyroxene (~1%). They are often associated with quartz-rich bands that form small intrafolial folds (Fig. 3a). Rocks from the Além Paraíba region (Fig. 3c and d) have a mineral assemblage dominated by feldspar (60–80%), quartz (20–30%), hornblende (~1%), and biotite (1–2%). They contain boudins of mafic composition that may reach up to 1 m in length, and decimeter-scale intrafolial folds. Rocks from the Santo Antônio de Pádua region (Fig. 3e and f) also contain high amounts of feldspar (~75%), and lesser modal amounts of quartz (15–20%), hornblende (~2%), biotite (~3%), and enstatite (~3%). They often contain folded quartz-rich layers that typically define a mylonitic transposition foliation (Fig. 3e). Accessory phases are mostly hematite, titanohematite, sillimanite, ilmenite and magnetite (< 1%).

4. Analytical methods

Microstructure characterization was carried out using optical and electron microscopes, focusing on grain shape, grain and phase boundaries, grain size, and deformation and reaction features. Quantitative microstructural analyses involving grain size distribution as well as textural aspects and crystal misorientation angles were performed using Mtex 4.0.16 tolbox in Matlab for crystallographic orientation data.

Crystallographic orientation measurements were obtained from automatically indexed EBSD patterns collected on a JEOL JSM 5600

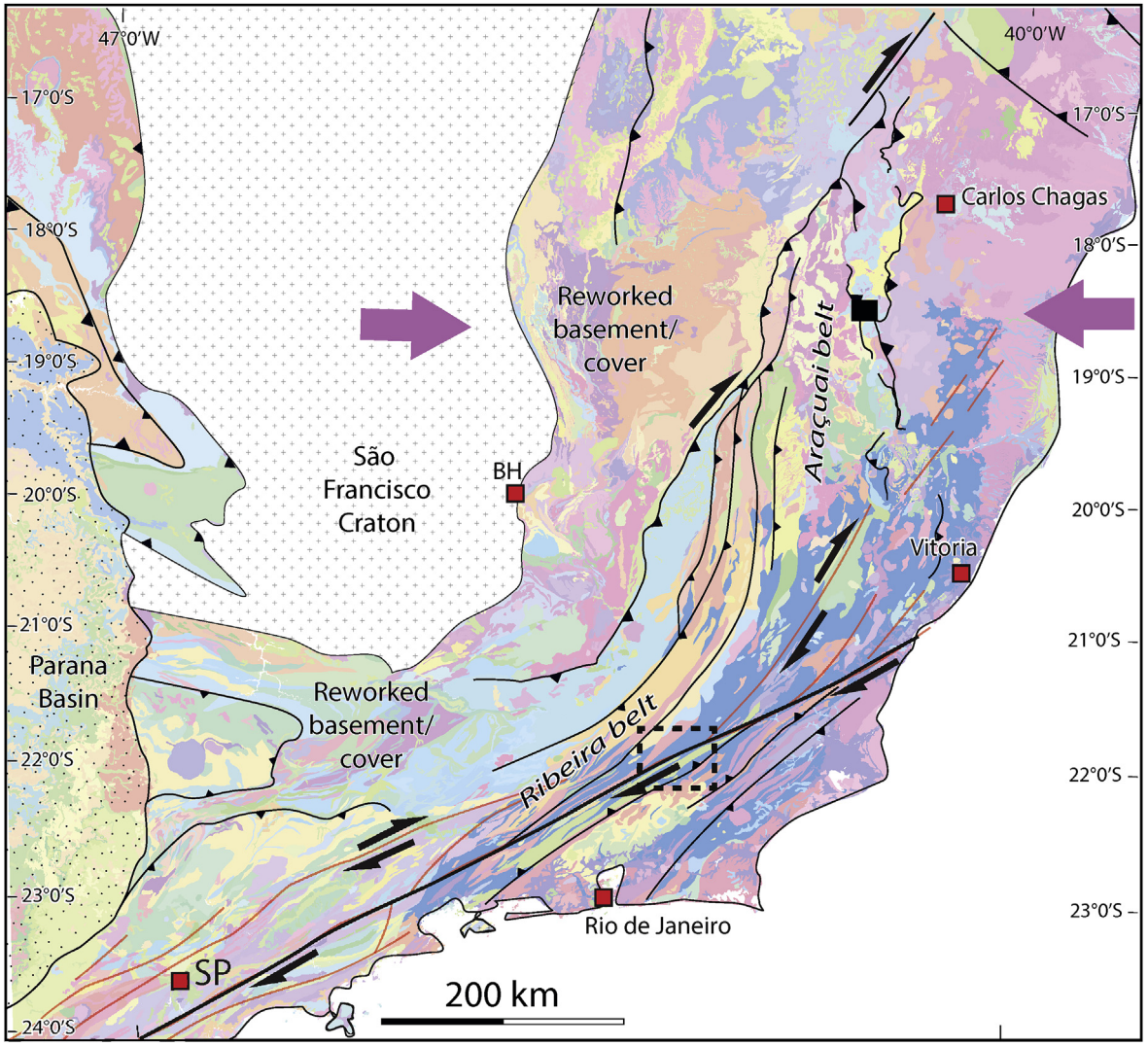

Fig. 1. Schematic geologic map of the Araçuaí-Ribeira belt compiled from public shapefiles from the Brazilian Geological Survey (CPRM) (http://geobank.cprm.gov.br). Purple arrows represent the E-W collision between South American and African continents. Red squares are cities. Dashed box represents the location of the study area. (For interpretation of the references to color in this figure legend, the reader is referred to the Web version of this article.)

SEM, equipped with an EBSD detector and HKL Technology's Channel 5 software package, at Géosciences-Montpellier (Université de Montpellier II-France). EBSD analyses were performed on thin sections cut perpendicular to the foliation (XY plane of finite strain), and parallel to the stretching lineation (X-direction). The sections were polished in colloidal silica for EBSD analysis. EBSD mapping was carried out on the whole thin section. Although all mineral phases were mapped, we here focus on quartz crystallographic textures, except for the grain size distribution analysis, which shows histograms for all the main mineral phases. Working conditions were as follows: 17 kV accelerating voltage, working distance of about 20 mm, 70° specimen tilt, and a step size ranging from 20 to 35 μm.

Misorientation angles between neighboring quartz grains have been grouped into: (1) low-angle boundaries, with misorientation of 2–10°, and (2) high-angle boundaries, with misorientation > 10°. The misorientation histograms were plotted from the mean grain orientation for grain segmentation with a minimum misorientation angle of 2°. Misorientation analysis of grain boundaries were performed for uncorrelated (random pairs) and correlated (neighbor pairs) distribution of angles and axes. Misorientation axes were plotted for specific angles ranging from 2 to 65°.

The Ti concentration in quartz was determined using a JEOL JXA – 8230 Electron probe micro analyzer equipped with five wavelength-dispersive X-ray spectrometers at Helmholtz-Zentrum Deutsches GeoForschungsZentrum (GFZ), Potsdam, Germany. Analytical procedures for EPMA analysis were analogous to those described in Armstrong (1995), which use the CITZAF X-ray correction program to convert X-ray intensity to concentration units, and the Armstrong PRZ algorithm for data correction. Working conditions were as follow: spot size 5–10 μm, spot spacing ranging between 70 and 110 μm, accelerating voltage 20 kV, and current 100 nA, which resulted in a detection limit of 7 ppm. A summary of quartz Ti content from Electron microprobe analysis is presented in Table 1, and the full data table is available in the supplementary material. Temperatures were calculated using the calibrations of Thomas et al. (2010) and Huang and Audétat (2012) by means of the following equations: Thomas et al. (2010).

$$T(°C) = \frac{a + cP}{b - R \times \ln X_{TiO_2}^{Qtz} + R \times \ln a_{TiO_2}} - 273.15 \quad (1)$$

where $a = 60.952$, $b = 1.520$, $c = 1.741$, R = gas constant (8.3145 J/mol K), T = temperature in Celsius, P = pressure in kbar, X_{TiO2}^{quartz} = mole fraction of TiO_2 in quartz and a_{TiO2} = activity of TiO_2 in the system. If the pressure can be constrained within ~1 kbar, the temperature can be estimated within ~20 °C. Huang and Audétat (2012)

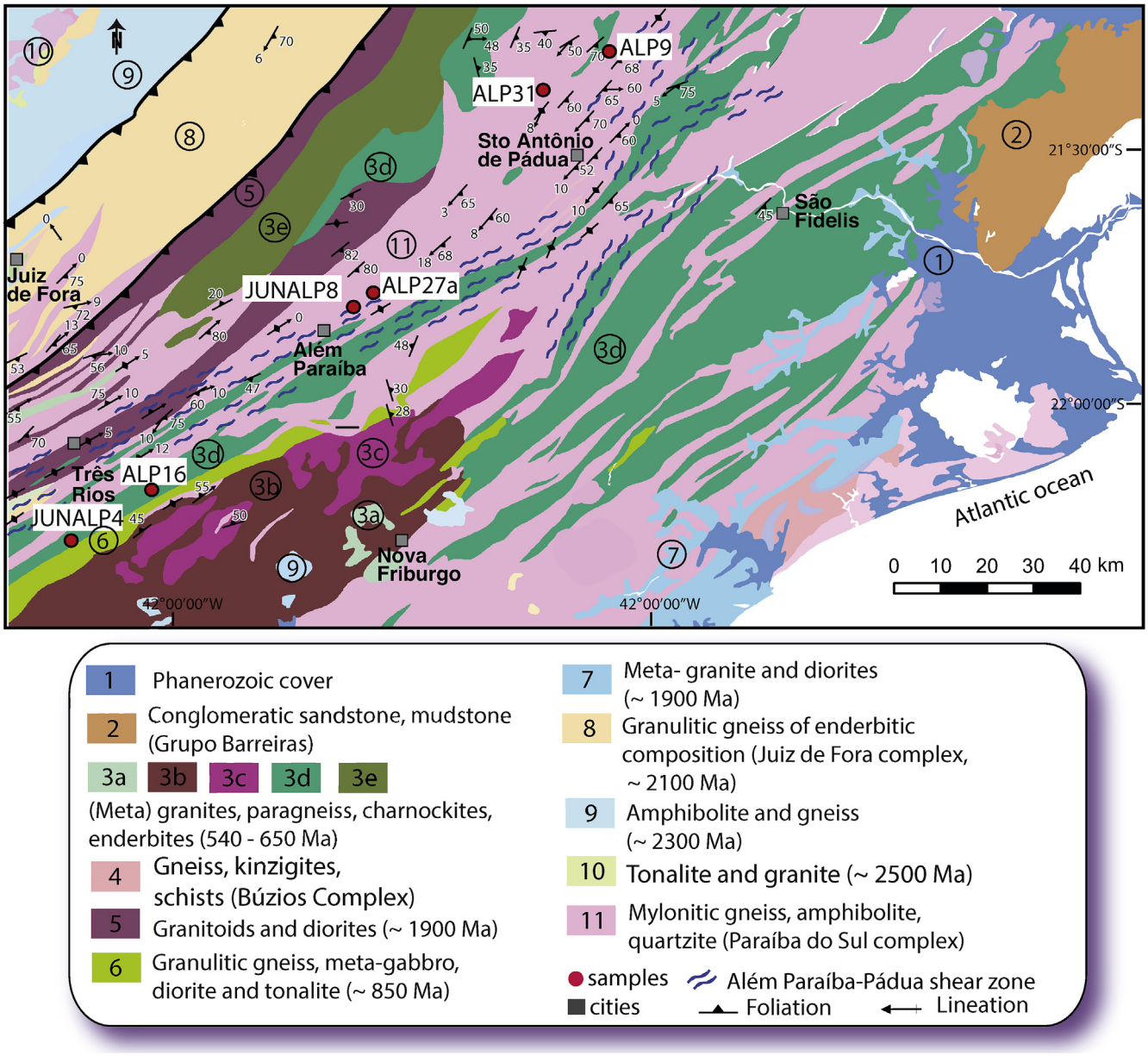

Fig. 2. Geologic map of the Três Rios-Além Paraíba-Pádua shear zone area, highlighting the location of the studied samples.

$$\log \mathrm{Ti(ppm)} = -0.27943\times10^4/T - 660.53(P^{0.35}/T) + 5.6459, \quad (2)$$

where T is given in Kelvin and P in kbar.

The a_{TiO2} in rutile-absent system such as the studied mylonites is expected to range from 0.6 to 1 (e.g., Ghent and Stout, 1984; Menegon et al., 2011; Cross et al., 2015). Based on the presence of ilmenite in our samples, we consider $a_{TiO2} = 0.6$ as suitable for our samples, although we also report TitaniQ temperatures for an activity of TiO_2 of 0.7 and 0.8, as proposed for other high-temperature mylonites (e.g., Cross et al., 2015). The results obtained using $a_{TiO2} = 0.6$ are considered as the maximum deformation temperatures at which quartz recrystallized, and the results obtained from activities of 0.7 and 0.8 are related to the minimum deformation temperatures. For a_{TiO2} errors of ± 0.2, temperature errors are at most ± 30 °C.

Prior to *in-situ* measurement of Ti in the EPMA, the samples were investigated using cathodoluminescence (CL) and backscattered electron images (BSE) to reveal any potential zoning in Ti concentration or any non-quartz impurities. BSE imaging was performed in a QUANTA 3D FEG scanning electron microscope (SEM) at the GFZ Helmholtz Centre, Potsdam, Germany. Working conditions for BSE images were as follows: operating conditions of 20 kV accelerating voltage, 8.0 nA beam current, and 9–10 mm working distance. Collection of CL imagery was performed using an Olympus BX41 microscope at Géosciences Montpellier, France.

5. Microstructures and grain-size distribution (GSD)

The different microstructural aspects of the high-temperature mylonitic rocks in the study shear zone segment are captured by the selection of thin sections shown in Fig. 4. These thin sections have been mapped by means of SEM-based EBSD analysis and are described in the following sections.

5.1. Três Rios region

Samples from the Três Rios region (JUNALP4 and ALP16) are characterized by grain sizes ranging from 80 to < 3500 μm, with recrystallized grains (80 to ≤ 500 μm in sizes) occupying between 50 and

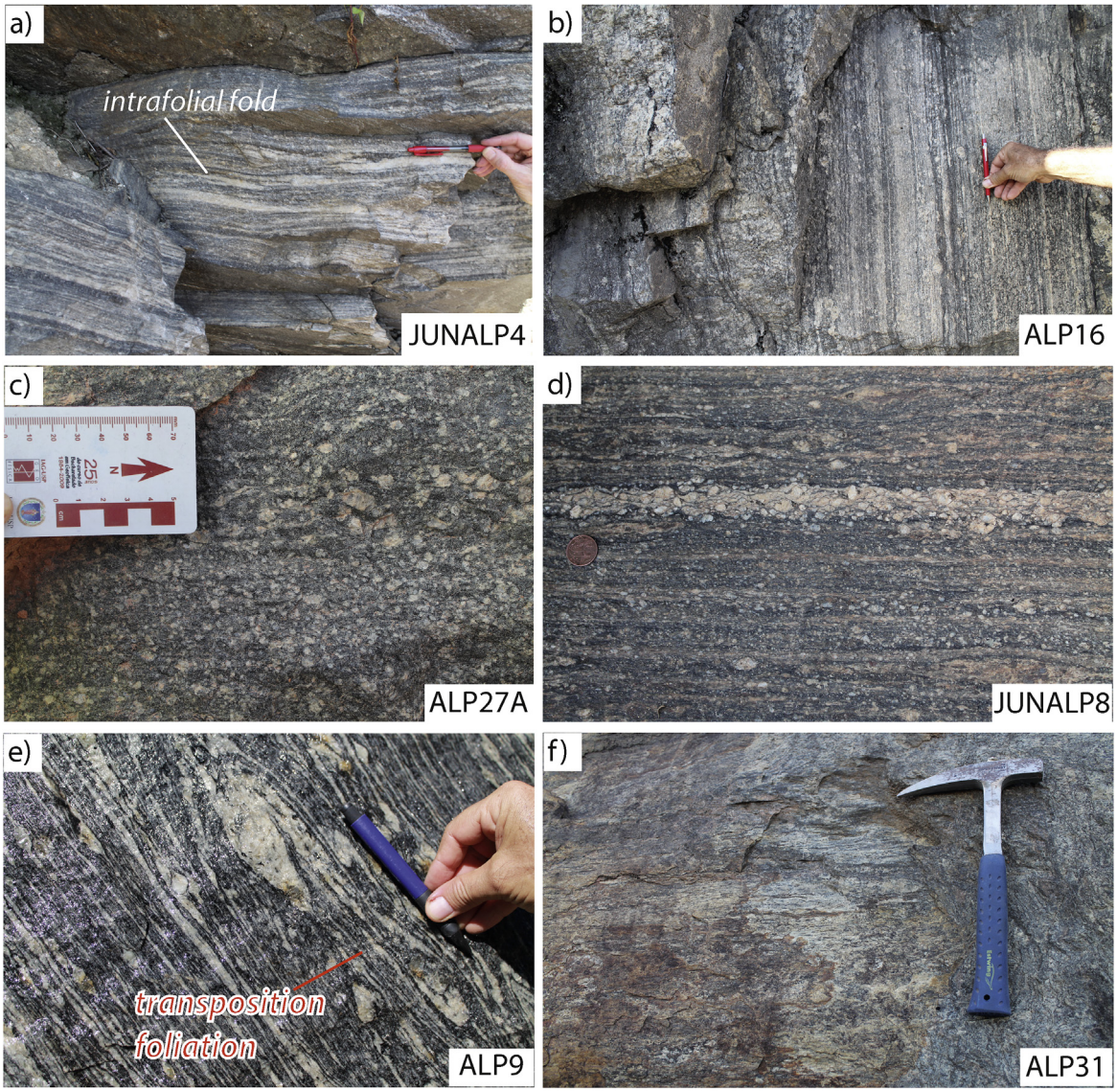

Fig. 3. Field photos of the studied rocks. (a) and (b) are mylonites derived from gneiss from the Três Rios region. (c) and (d) are feldspar-rich mylonites from the Além Paraíba region. (e) and (f) are mylonitic rocks from the Santo Antônio de Pádua region showing mylonitic transposition foliation (e).

80% of the total rock volume (Figs. 4–6). The main peaks of grain sizes range from 150 to 250 μm (Fig. 6), and the recrystallized grains occur in a frequency ranging from 15 to 25%.

Quartz occurs as large and thin discontinuous ribbons with aspect ratios varying from 4:1 to 13:1, often associated with orthoclase rich domains (Fig. 5a–c), and forms cusps that point into feldspar porphyroclasts. Quartz frequently displays irregular and smooth grain boundaries, undulose extinction, and subgrain boundaries (Figs. 5a and b and 7). Quartz grain boundaries in the ribbons tend to be perpendicular to the long axis of the ribbons (Figs. 5b and c and 7a). Some large quartz grains (~3 mm long) that wrap around andesine porphyroclasts have chessboard subgrain optical extinction patterns (Fig. 5a and b). Few quartz grains of granular shapes occur in the amphibole-feldspar rich matrix (Fig. 5d).

Feldspar (orthoclase and andesine) occurs as 1–4 mm long porphyroclasts that exhibit undulose extinction, subgrain boundaries, deformation twins, and mantle-core structures (Fig. 5b and c). Some large orthoclase porphyroclasts (~3.5 mm in diameter) with only faint undulose extinction display a mantle of much smaller grains around their rims (Fig. 5c), and have inclusions of strain free quartz and biotite (Fig. 5b). The smaller feldspar grains (100–200 μm in size) form domains of recrystallized aggregates with straight grain boundaries in an array of polygonal microstructure (Fig. 5a).

Hornblende occurs as rounded or elongated porphyroclasts with sizes ranging from > 0.7 to ~2.2 mm, or as more or less equant grains in the matrix, with sizes varying from 90 to 400 μm. These recrystallized grains in the matrix display irregular lobate grain boundaries, frequently associated with recrystallized feldspar grains (Fig. 5d).

Orthopyroxene (enstatite) occurs as elongated crystals (Fig. 5j), particularly associated with biotite and hornblende. Orthopyroxene displays granular shapes and sizes of ~100 μm arranged in irregular lobate boundaries. Biotite exhibits light brown and strong red colors in tabular shapes and sizes varying from 100 to 500 μm with a strong shape-preferred orientation.

5.2. Além Paraíba region

Rocks from this region (ALP27a and JUNALP8; Fig. 4) have grains sizes ranging from 20 μm to 1.8 mm. The recrystallized grains (most 50–500 μm) represent approximately 80% of the total rock volume with a dominant grain size of 80–120 μm, which occur with a frequency between 35 and 50% (Figs. 4 and 6).

Table 1
Summary of Ti content results and respective temperature calculations using calibrations from Huang and Audétat (2012) and Thomas et al. (2010).

Sample ID	[a]Ti (ppm)	T °C Huang and Audétat (2012)	T °C - Thomas et al. (2010)	T °C - Thomas et al. (2010)	T °C- Thomas et al. (2010)
			a = 0.6/P = 6.5 Kbar	a = 0.7/P = 6.5 kbar	a = 0.8/P = 6.kbar
Sto Antônio de Pádua region					
ALP9 (QTZ 4)	51	759	659	643	631
ALP9 (QTZ 4)	92	831	721	704	689
ALP 9 (QTZ 6)	58	775	672	656	643
ALP 9 (QTZ 6)	119	866	752	734	718
ALP31 (QTZ 1)	43	739	641	626	614
ALP31 (QTZ 1)	115	861	748	730	714
ALP31 (QTZ 5)	42	738	640	625	613
ALP31 (QTZ 5)	105	849	737	719	704
ALP 31 (QTZ 1a)	49	755	655	640	627
ALP 31 (QTZ 1a)	73	802	696	680	666
ALP 31 (QTZ 2)	59	777	674	658	645
ALP 31 (QTZ 2)	87	824	715	698	684
ALP 31 (QTZ 3)	74	803	697	681	667
ALP 31 (QTZ 3)	124	872	757	738	723
ALP 31 (QTZ 4)	52	761	660	644	632
ALP 31 (QTZ 4)	70	796	691	674	661
ALP 31 (QTZ 5)	61	780	677	661	648
ALP 31 (QTZ 5)	76	806	700	683	669
ALP 31 (QTZ 6)	58	775	672	656	643
ALP 31 (QTZ 6)	71	798	692	676	663
Além Paraíba region					
ALP27a (QTZ 1)	35	719	623	609	598
ALP27a (QTZ 1)	59	776	673	657	644
ALP27a (QTZ 4)	29	698	605	591	580
ALP27a (QTZ 4)	119	865	751	733	718
JUNALP8 (QTZ 1)	29	698	605	591	580
JUNALP8 (QTZ 1)	53	765	663	648	635
JUNALP8 (QTZ 2)	44	744	645	630	618
JUNALP8 (QTZ 2)	62	783	679	663	650
Três Rios region					
APL16 (QTZ 1)	22	673	582	569	559
APL16 (QTZ 1)	36	721	625	611	599
APL16 (QTZ 2)	25	685	593	580	569
APL16 (QTZ 2)	56	771	669	653	640
JUNALP4 (QTZ 1)	33	712	617	603	591
JUNALP4 (QTZ 1)	52	762	661	646	633
JUNALP4 (QTZ 2)	34	716	620	606	595
JUNALP4 (QTZ 2)	44	742	644	629	617
JUNALP4 (QTZ 3)	36	721	625	611	599
JUNALP4 (QTZ 3)	46	748	649	634	621
JUNALP4 (QTZ 4)	25	685	593	580	569
JUNALP4 (QTZ 4)	31	706	612	598	587
JUNALP4 (QTZ 5)	22	670	580	567	557
JUNALP4 (QTZ 5)	42	738	640	625	613
JUNALP4 (QTZ 6)	35	719	623	609	598
JUNALP4 (QTZ 6)	44	744	645	630	618
JUNALP4 (QTZ 1a)	24	680	589	576	565
JUNALP4 (QTZ 1a)	38	726	630	615	603
JUNALP4 (QTZ 3a)	24	680	589	576	565
JUNALP4 (QTZ 3a)	38	726	630	615	603

[a] Minimum and maximum Ti content in each single grain.

Quartz occurs mainly as polycrystalline continuous and discontinuous ribbons with aspect ratios varying from 10:1 to 22:1. Some augen-shaped ribbons have aspect ratios around 5:1 (Fig. 5e and f). The ribbons often display irregular, smooth to lobate boundaries, but straight grain boundaries are also observed, particularly in the continuous ribbons. Discontinuous ribbons contain undulose extinction and subgrains, while evidence of crystal-plastic deformation in continuous ribbons is scarce.

Feldspar occurs as porphyroclasts or forming domains of recrystallized grains. Porphyroclasts have sizes between 1 and ~3.5 mm, and typically contain inclusions of quartz and biotite (Fig. 5e). Partially recrystallized andesine porphyroclasts display a mantle of recrystallized grains and deformation bands (Fig. 5g). The feldspar grains in the recrystallized mantles are very fine-grained, with grain sizes around 20 μm (Fig. 5g). Orthoclase porphyroclasts display weak undulose extinction and subgrain boundaries (Fig. 5h). They have irregular lobate boundaries and their rims are partly recrystallized (Figs. 5h and 7b,c).

Hornblende occurs as elongated or augen-like porphyroclasts. They have sub-to anhedral shapes and sizes varying from ~0.8 to 1.5 mm (Fig. 5f and h). Light brown biotite shows subhedral shapes, sizes varying from 200 to 1000 μm, and is often associated with titanohematite and magnetite. Biotite grains show a strong shape-preferred orientation, which characterizes foliation domains that typically wraps around porphyroclasts. Sillimanite is associated with recrystallized feldspar grains and biotite in narrow bands (Fig. 5e).

5.3. Santo Antônio de Pádua region

Rocks from this region (ALP9 and ALP31; Fig. 4; Fig. 5i–l) contain

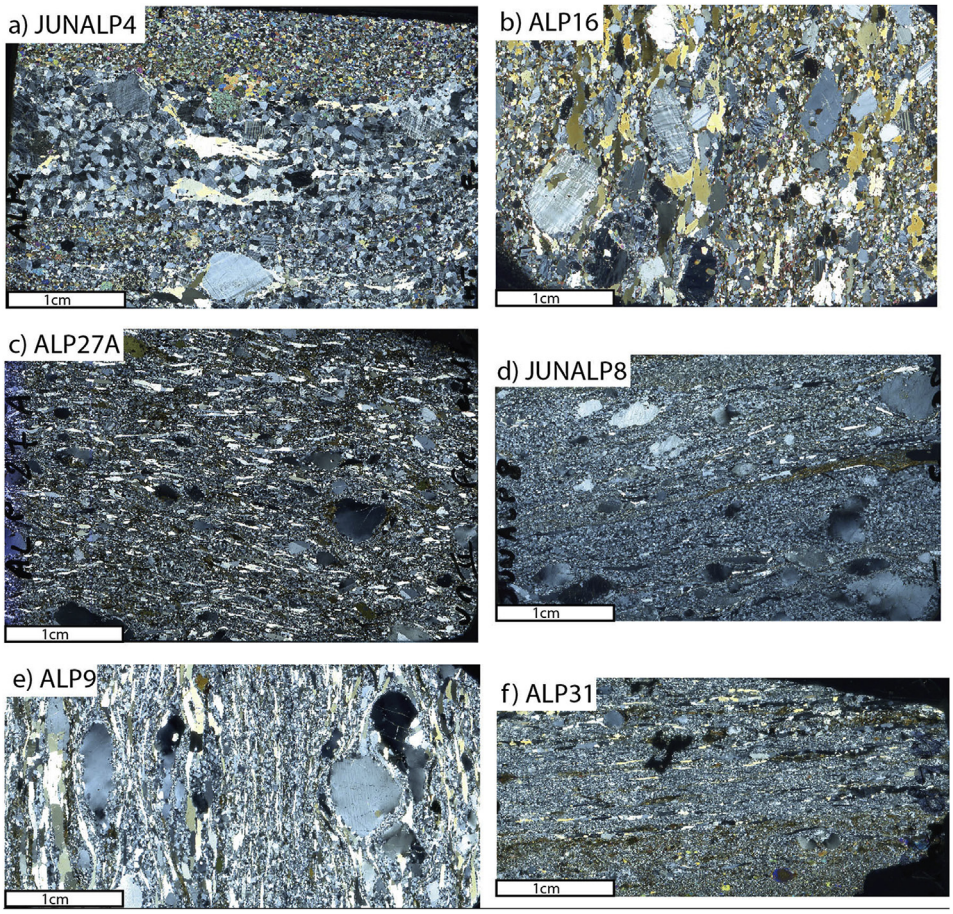

Fig. 4. Images of scanned thin sections (crossed polars) from the studied samples from Três Rios (JUNALP4 and ALP16), Além Paraíba (ALP27A and JUNALP8), and Santo Antônio de Pádua (ALP9 and ALP31), displaying the general aspect of the microfabrics and grain size domains.

grains with sizes between ~30 μm and 2.8 mm. They are characterized by alternating quartz ribbons and mafic layers. The percentage of recrystallized grains is between 50 (ALP9) and 90% (ALP31) and grain size peaks at 80–100 μm (Fig. 6c) in frequencies of 30 and 45%.

Quartz occurs mainly as polycrystalline ribbons with aspect ratios ranging from 6:1 to 23:1. Ribbons often have irregular, smooth to lobate boundaries (Fig. 5i–l), faint undulose extinction and are almost devoid of subgrains.

Feldspar grains in recrystallized domains have sizes ranging from 30 to ~350 μm. Orthoclase porphyroclasts display rounded and elongate shapes (augen), myrmekite, subgrain boundaries, mantle-core structures and undulose extinction (Fig. 5k). Some porphyroclasts are completely recrystallized, consisting of aggregates of grains with sizes up to 100 μm. Andesine porphyroclasts vary in size from 1200 to 6000 μm, show rounded shapes, deformation twins and undulose extinction, and are substantially recrystallized (Fig. 5i).

Hornblende occurs as rounded or elongated porphyroclast with diameters ranging from 500 to 1800 μm. Recrystallized hornblende has grain sizes in the range of 50–100 μm and occurs in the matrix together with feldspar (Fig. 5i). Grain boundaries are essentially irregular.

Biotite crystals are dark to light brown and red in color, as observed in plane-polarized light. The elongated grains have a well-developed shape fabric with a size range of 70–600 μm, some of them showing augen shapes (Fig. 5i). Orthopyroxene occurs as elongated porphyroclasts with sizes around 1400 μm, typically wrapped by polycrystalline quartz ribbons, or as anhedral grains with sizes ranging from 50 to 400 μm (Fig. 5j).

6. CPO fabric

The quartz CPO data are presented in Fig. 8. In general, the fabrics are weak, with a J-index ranging from 1.1 to 3.6, and with evidence of activation of several slip systems.

6.1. Três Rios region

Quartz CPOs from samples of this region (ALP16 and JUNALP4) display two patterns. Quartz from ALP16 has a main concentration of < c > axes close to X (Fig. 8a–b), consistent with prism < c > slip and dextral sense of shear. Poles to {10-10} and < a > exhibit similar textures with distribution along great circles and with maxima close to Z (normal to foliation) (Fig. 8a). Rhomb planes {01–11} and {10–11} have maxima in the SW quadrant and close to Y, respectively. A secondary distribution of the positive rhombohedral {r} poles occurs around the Z-axis of the pole figure, i.e. around the foliation normal. However, the most prominent texture in this sample indicates slip along the {m} planes parallel to the c-axis.

Quartz from JUNALP4 has a different CPO pattern, with a small-circle distribution of < c > axes that is located at ~40° to Z (Fig. 8b). The poles to {10-10} define a great circle with a main maximum close to Y. The poles to the rhomb planes {01–11} and {10–11} have two main maxima close to Z, and two less prominent maxima. The < a > poles have a maximum at a small angle to the foliation plane halfway between Y and X (Fig. 8b). In contrast to ALP16, the highest concentrations of crystallographic poles are consistent with rhomb planes that may have acted as the main slip planes, together with prism planes.

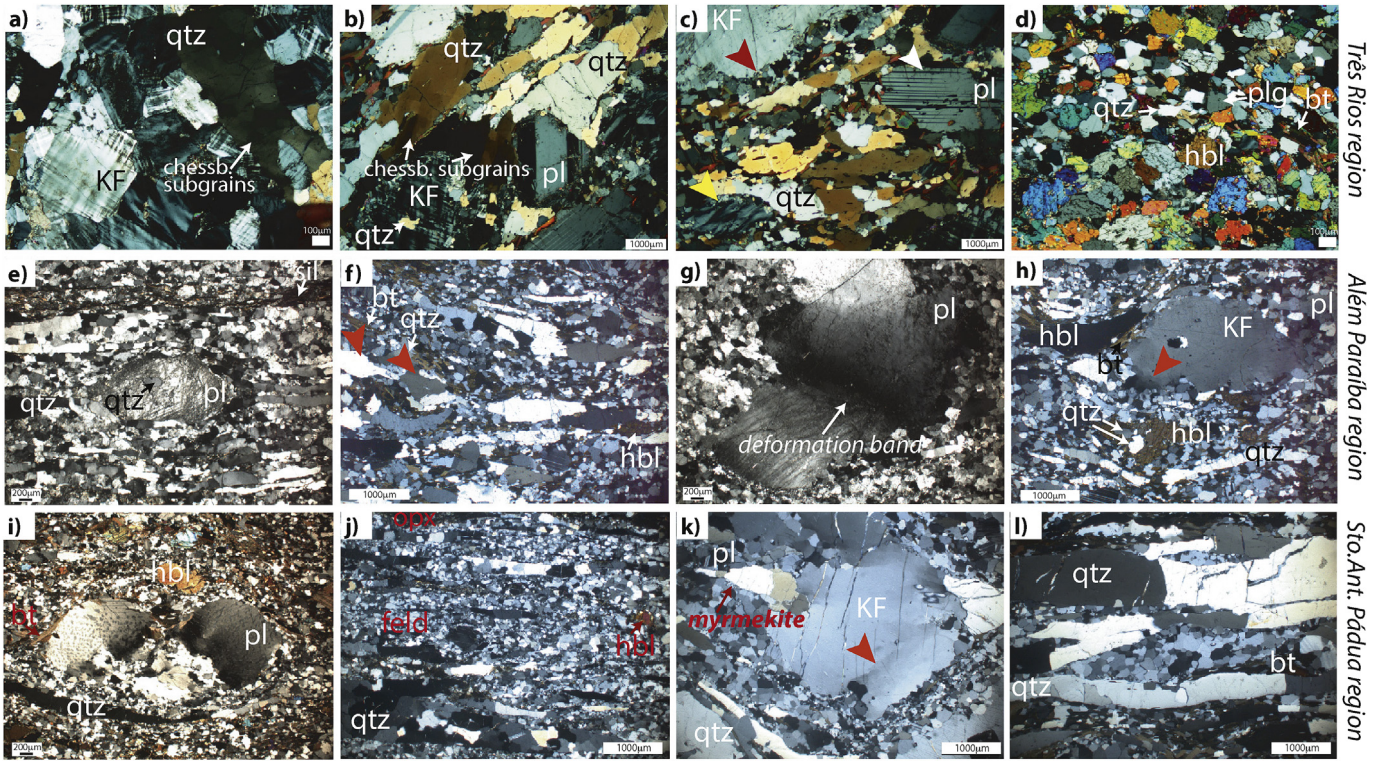

Fig. 5. Microstructural aspects of representative high-temperature mylonites. Feldspar porphyroclasts displaying undulose extinction and polygonal shapes (a) are surrounded by large quartz ribbons exhibiting chessboard subgrain boundaries (b and c; red arrow points to independent new grain in the rim of the weakly deformed feldspar porphyroclast, white arrow points to deformation twins in plagioclase, and yellow arrow points to recrystallized mantle in feldspar); (d) granular quartz grains associated with amphibole-feldspar rich matrix; (e) porphyroclasts of feldspar with quartz inclusions and silimanite-rich band associated with recrystallized feldspar domain; (f) quartz ribbons with "augen" shape (red arrows); (g) partially recrystallized andesine porphyroclast displaying mantle of recrystallized grains and deformation bands; (h) orthoclase porphyroclast displaying weak undulose extinction and subgrain boundaries (red arrow points to subgrain boundaries) and hornblende porphyroclasts; (i) andesine porphyroclast partially recrystallized and hornblende porphyroclast associated with feldspar in the matrix; (j) elongated orthopyroxene associated with recrystallized feldspar domain; (k) partly recrystallized orthoclase porphyroclast displaying subgrain boundaries (red arrow) and myrmekite structure; (l) polycrystalline quartz ribbons showing irregular smooth and lobate boundaries. (For interpretation of the references to color in this figure legend, the reader is referred to the Web version of this article.)

6.2. Além Paraíba region

Quartz CPO from samples from the Além Paraíba region (JUNALP8 and ALP27a) have < c > axes that define a single maximum close to X consistent with dextral sense of shear (JUNALP8; Fig. 8c) or at ~40° to X, possibly indicating sinistral sense of shear (ALP27a; Fig. 8d). Poles to prism {m} of JUNALP8 define a broad great circle with a maximum close to Z (Fig. 8c). A similar broad girdle is observed for < a > axes (Fig. 8c). Poles to z-rhomb planes form symmetrical small maxima ~45° to X or to Z (Fig. 8c), and poles to r-rhomb display a main concentration close to X or ~45° to X or Z (Fig. 8c). Prism {m} poles of ALP27a form a broad skeleton girdle with a main cluster close to Y. < a > axes define a similar skeleton girdle, but with two maxima located between Z and Y (Fig. 8d). Poles to r-rhomb planes have a main concentration close to Z, while z-rhomb poles cluster between Y and X (Fig. 8d). In general, the JUNALP8 CPO diagrams are similar to ALP16, again suggesting the presence of prism < c > slip, while ALP27a CPOs are more indicative of a rhomb slip, which can be deduced from the maximum of {r} poles near the Z-axis of the sample.

6.3. Santo Antônio de Pádua region

Quartz CPO from samples of Santo Antônio de Pádua (ALP9 and ALP31) feature a [c]-axis maximum in the XZ plane at a small angle (20–30°) to X (Fig. 8e and f), plus asymmetric girdles of poles to {m} planes that run from northwest to southeast, with a maximum close to Y. < a > axes are also distributed in a girdle that runs from north to south, with two main maxima close to Y. Poles to rhomb {r} and {z} planes have some clusters between Y and Z, Y and X, at ~30° to Z, and close to X, Y and Z. They show a more or less square pattern with a somewhat symmetrical distribution. The CPO patterns of ALP31 in many ways look similar to ALP27a.

6.4. Summary of the CPO fabrics

In general, all the samples have c-axes near the X-direction of the pole figures. All samples with this characteristic also have distributions of < a > and {m} poles along great circles whose poles approach the Z-axes (pole to foliation) of the samples. Additional slip on rhombohedral planes is possible where, except for ALP31, all samples have at least one secondary maximum close to the foliation normal.

7. Misorientation angle analysis

The misorientation between two adjacent grains is defined by the rotational operation that makes one crystal lattice coincide with the other. Hence the misorientation is described by a rotation angle about an axis of rotation, known as the misorientation angle and the corresponding misorientation axis (Lloyd et al., 1997; Wheeler et al., 2001; Lapworth et al., 2002). Quartz misorientation angle histograms for all our samples exhibit two distinct maxima (Fig. 9a–f), except for sample JUNALP8, which displays just one (Fig. 9d). The misorientation axes were plotted from the intervals observed in the misorientation angle distribution. A first sharp peak occurs at very low angles (~5°) and a

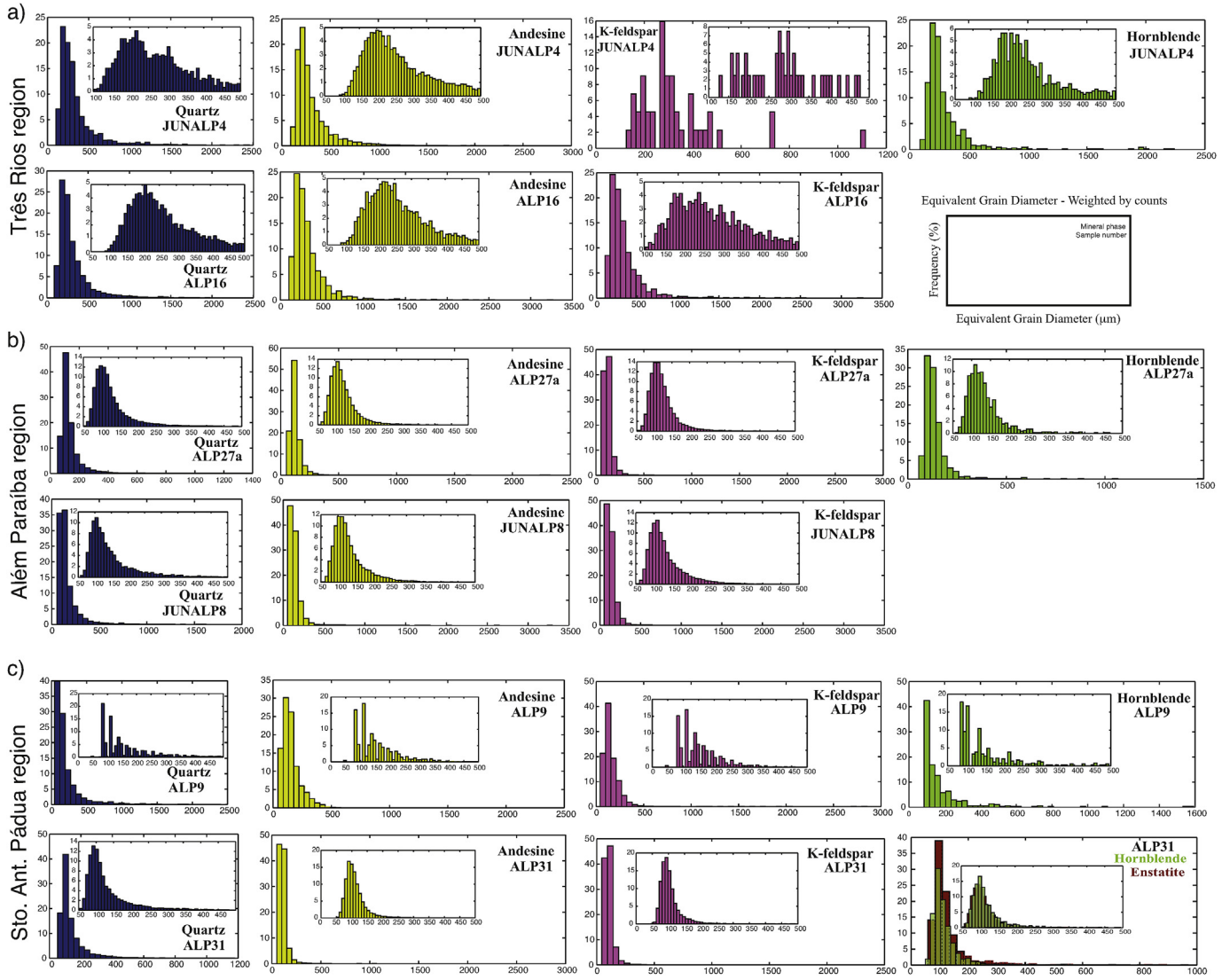

Fig. 6. Grain size distribution diagrams for quartz for the six samples studied in this work.

second one at 55–60°. Angles up to 20° are related to subgrains and recrystallized grains. The rotation axes tend to be aligned parallel to [0001]. Similarly, the misorientation axes for the misorientation angles in the interval 55–60° are oriented parallel to [c]. This is explained by Dauphiné twinning, where quartz crystals are rotated 60° about the [c] axis (Fig. 9a–f). Additionally, misorientation angles of 10–40° occur with higher frequency than expected for a uniform distribution, whereas misorientations greater than 60° occur with a lower frequency than expected for a uniform distribution.

In addition to the two main maxima of misorientation axes at 5 and 60°, there is a broad distribution in the interval between 10 and 20°. In detail, there is more than one maximum within this interval, which suggests that these grains were plastically deformed via the operation of multiple slip systems. It should also be noticed that in the 60–65° range some samples have rotation axes for the slip system {r} < a > , confirming the observation from the pole figures where poles to the rhomb planes {r} concentrate near the Z-axis of the samples (Fig. 8). The maxima for the misorientation axes parallel to the c-axis may also indicate activity of the prism slip system {m} < a > . However, no maximum is observed around the Y-axis in the pole figure plots. Therefore, these are again interpreted as a rotation around the c-axis caused by Dauphiné twinning.

8. TitaniQ temperature estimates

Ti concentrations were measured at 320 spots in 2–6 quartz grains from each sample. All the analyzed quartz grains show some evidence of intracrystalline deformation, such as undulose extinction and/or subgrains. They form continuous or discontinuous quartz ribbons. The EPMA spots were performed along longitudinal and transverse profiles across each quartz grain. The analytical spots were selected away from inclusions, other mineral phases and fractures. Evaluation of CL intensity showed a homogeneous light blue color, without evidence of zoning (see supplementary material).

Ti content and the temperatures obtained using the Thomas et al. (2010) and Huang and Audétat (2012) calibrations are presented in Figs. 10 and 11 and Table 1. Measurements show that the Ti content is heterogeneously distributed throughout individual quartz grains, but remarkably similar average concentrations are observed between grains from the same sample (variation ≤15 ppm; except the samples ALP9 and ALP31 from Sto Antônio de Pádua, for which the average variation ranges from 18 to 20 ppm, respectively), and between samples from the same region (variation of 2 ppm in Três Rios, 7 ppm in Além Paraíba, and 22 ppm in Sto. Antônio de Pádua; Table 1). The average Ti content increases from the southwest to the northeast, with values from 31 (ALP16) to 33 ppm (JUNALP4) in Três Rios, 47 (JUNALP8) to 54 ppm

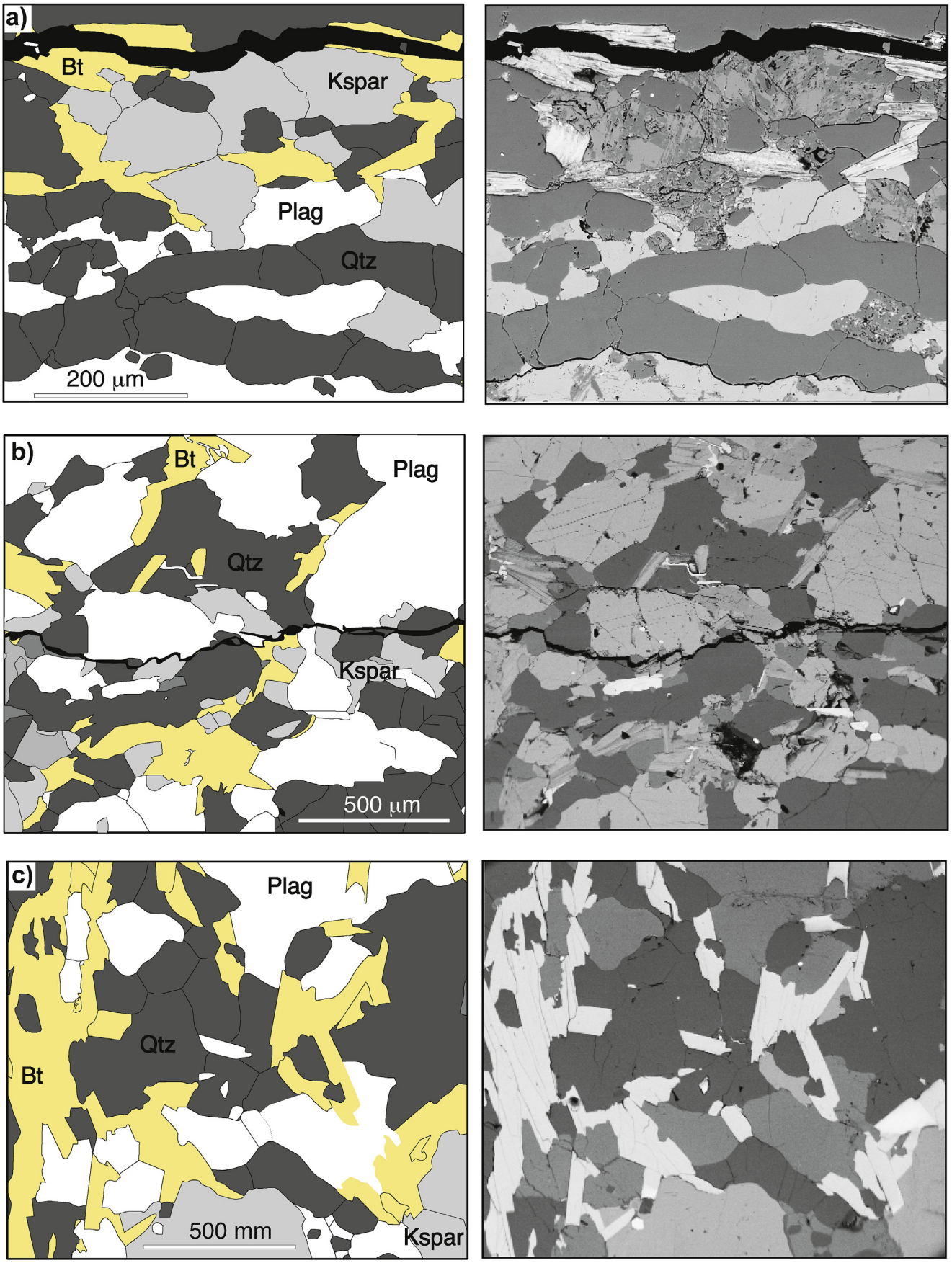

Fig. 7. Backscatter images of the mylonitic rocks (right) and schematic sketches (left). (a) Quartz-quartz grain boundaries in ribbon grains oriented perpendicular to the long axis of the ribbons. (b) and (c): predominantly irregular lobate grain boundaries between quartz, feldspar and biotite.

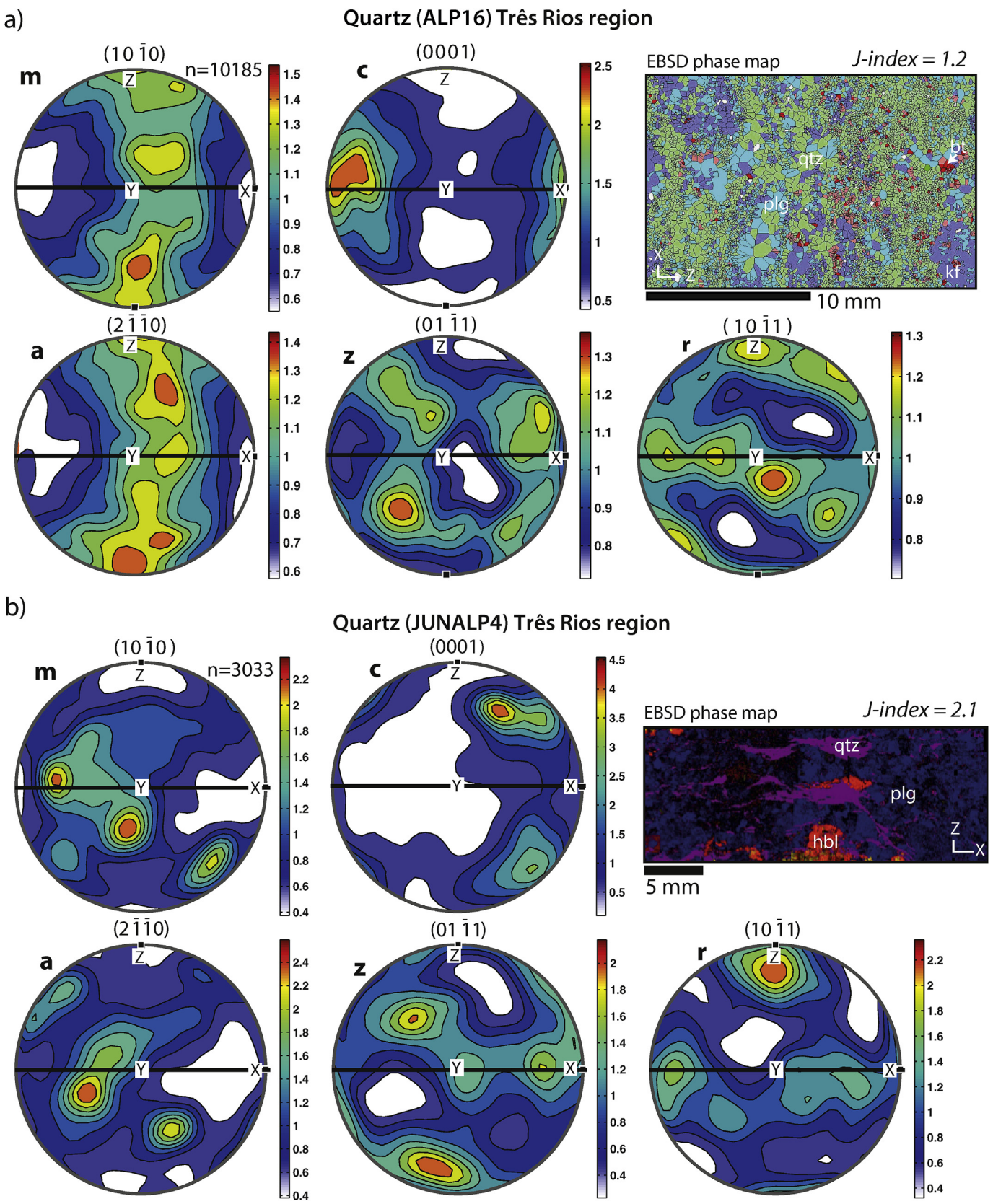

Fig. 8. Pole figures of quartz crystallographic orientation data (equal area, lower hemisphere projections; XZ sections of strain ellipsoid) and EBSD phase maps for the rocks from the Três Rios (a and b), Além Paraíba (c and d), and Santo Antônio de Pádua (e and f) regions. The maximum density distribution of [c]-axes is 7 times uniform (value in upper right corner).

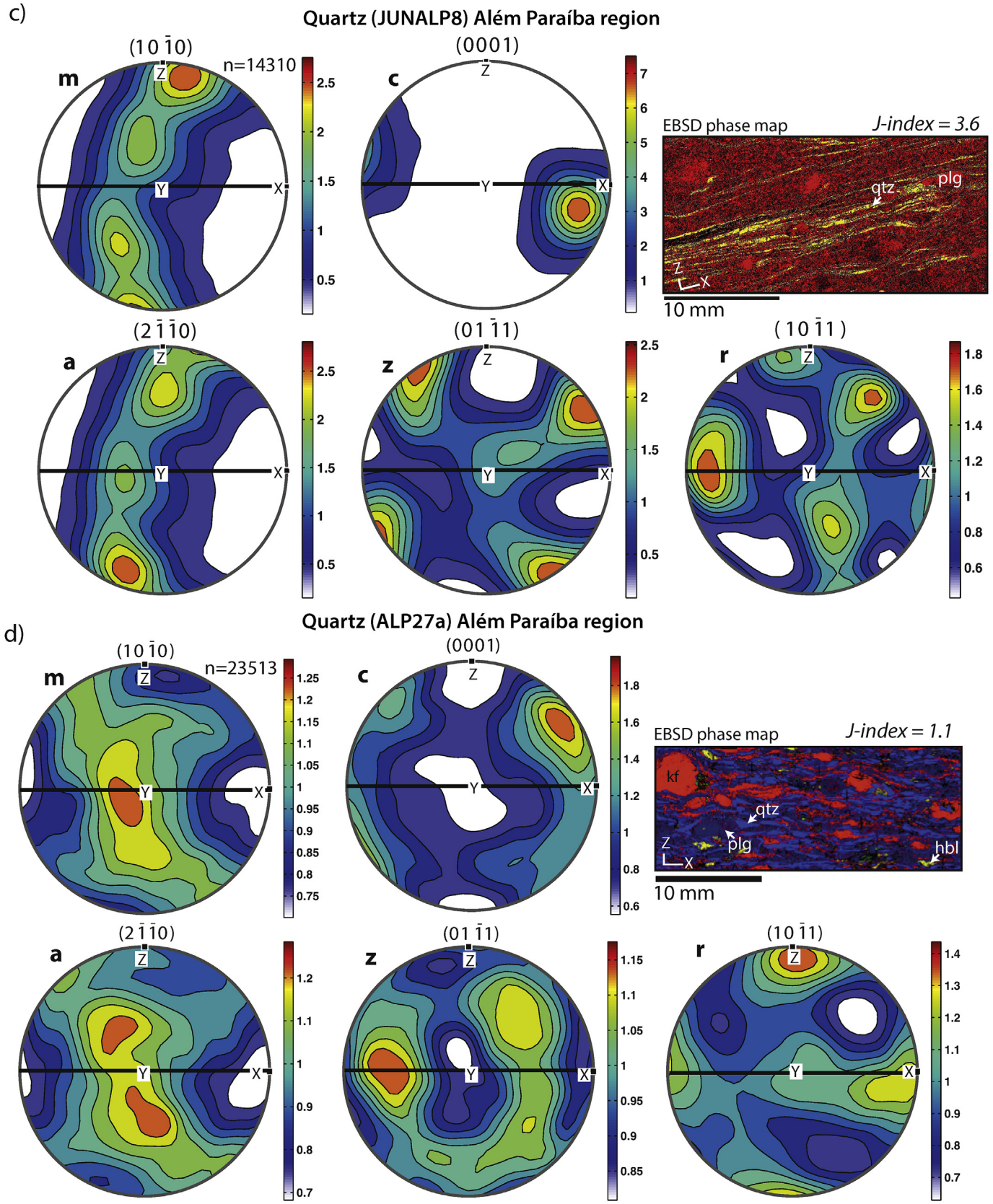

Fig. 8. (*continued*)

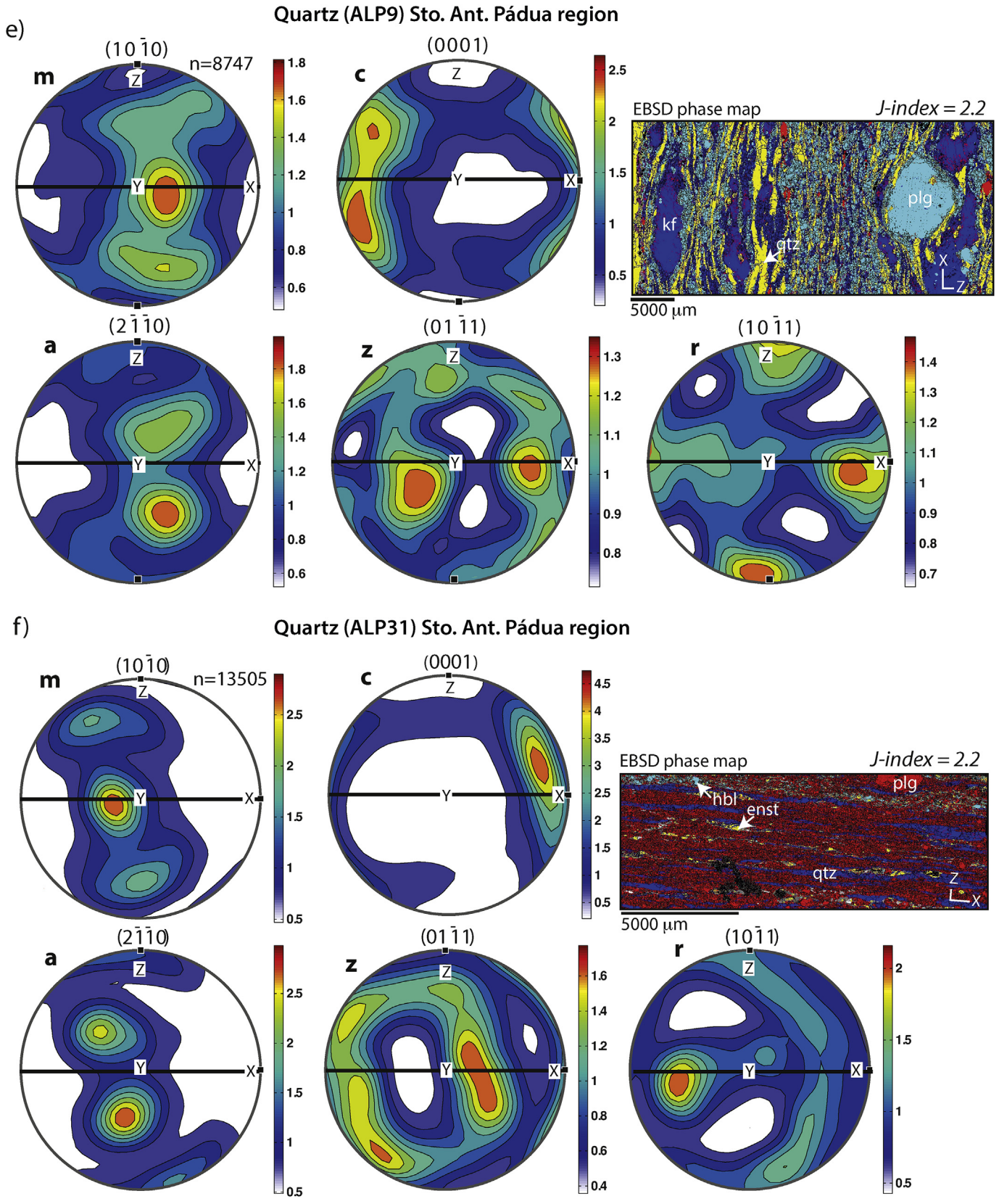

Fig. 8. (*continued*)

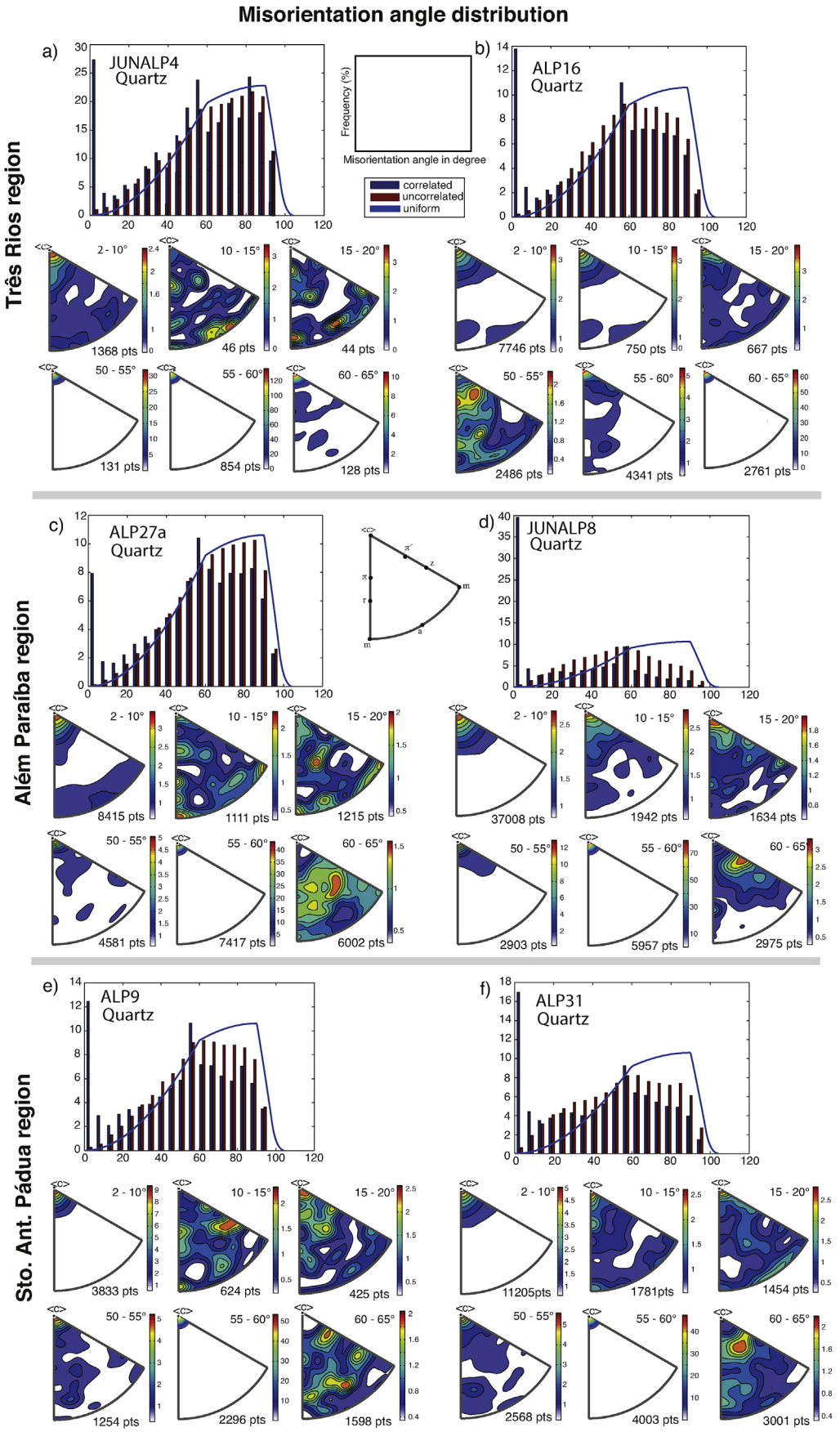

Fig. 9. Histogram of frequency of misorientation angles and misorientation axis/angle for quartz in samples from Três Rios (a and b), Além Paraíba (c and d), and Santo Antônio de Pádua regions (e and f).

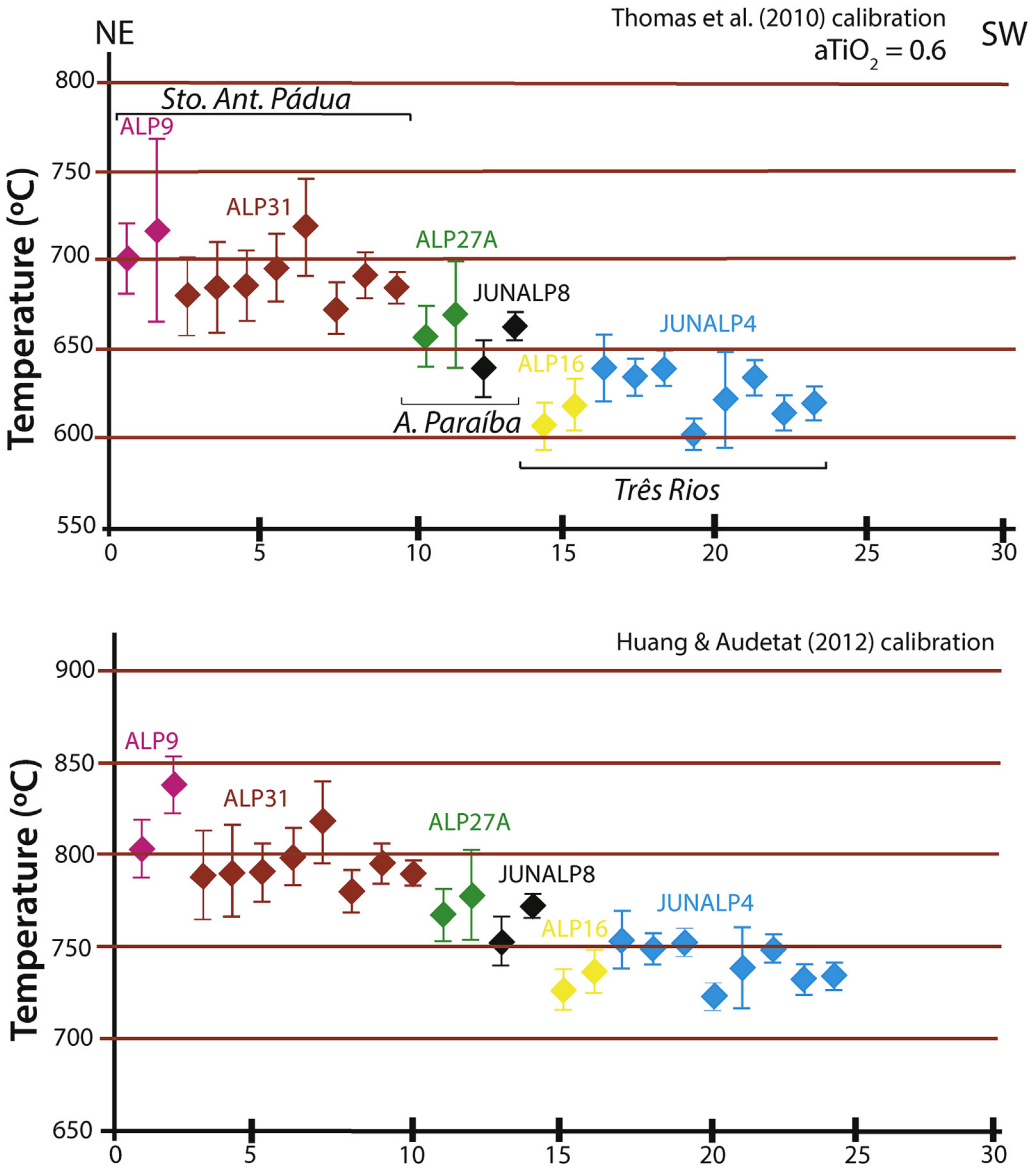

Fig. 10. TitaniQ temperature estimates for quartz in the studied rocks using both calibrations discussed in the text. The X-axis represents the number of grains.

(ALP27a) in Além Paraíba, and 65 (ALP31) to 87 ppm (ALP9) in Sto. Antônio de Pádua. We found no clear difference in Ti content between rims and cores of individual quartz ribbons (Fig. 11).

The calculated average temperatures using both calibrations exhibit a gradient, with the lower temperatures in Três Rios region and the higher temperatures in Sto. Antônio de Pádua region. The average temperatures using Thomas et al. (2010) calibration are 612–618 °C in Três Rios, 650–665 °C in Além Paraíba, and 682–739 °C in Santo Antônio de Pádua (Figs. 10 and 12). The average temperatures calculated using the Huang and Audétat (2012) calibration range from 705 to 712 °C in Três Rios, 748–763 °C in Além Paraíba, and 786–822 °C in Sto. Antônio de Pádua. The errors are around ± 20 °C (Figs. 10 and 12).

9. Comparison of Ti calibrations

Currently, two calibrations for the *P-T* dependence of Ti solubility in quartz have been applied to constrain temperature conditions during quartz (re-)crystallization: Thomas et al. (2010), which includes the original calibration of Wark and Watson (2006), and Huang and Audétat (2012). These calibrations often yield significantly different *P-T* estimates (e.g., Cavalcante et al., 2014; Nachlas et al., 2014; Cross et al., 2015). In the three studied regions the average temperatures obtained using Huang and Audétat calibration, as observed in previous studies, are ~80–100 °C higher (Fig. 12) than those obtained using Thomas et al. (2010). Such a great difference is independent of the Ti concentration in each region. Although Thomas et al. (2015) suggested that this difference is due to a lack of equilibrium in experimental conditions in the Huang and Audétat (2012) calibration, it is still unclear what fundamental process is responsible for the differences between these two calibrations, and how this pertains to the application of the TitaniQ geothermobarometer in crustal rocks.

The recent work by Thomas et al. (2015) suggests that the large variation in Ti concentration of quartz observed by Huang and Audétat (2012) may be related to gradients in Ti activity that persisted throughout each of their experiments, because their Ti-free quartz starting material always coexisted with Ti-rich quartz. Thomas et al. (2015) also mention that the lack of rutile in Huang and Audétat's experiments might also be attributed to incomplete $aTiO_2$ buffering. Thomas et al. (2015) therefore concluded that equilibrium solubilities of Ti in quartz likely were not achieved during Huang and Audétat's experiments at any given *P-T* condition. A non-chemical equilibrium condition during their experiments would affect the fundamental

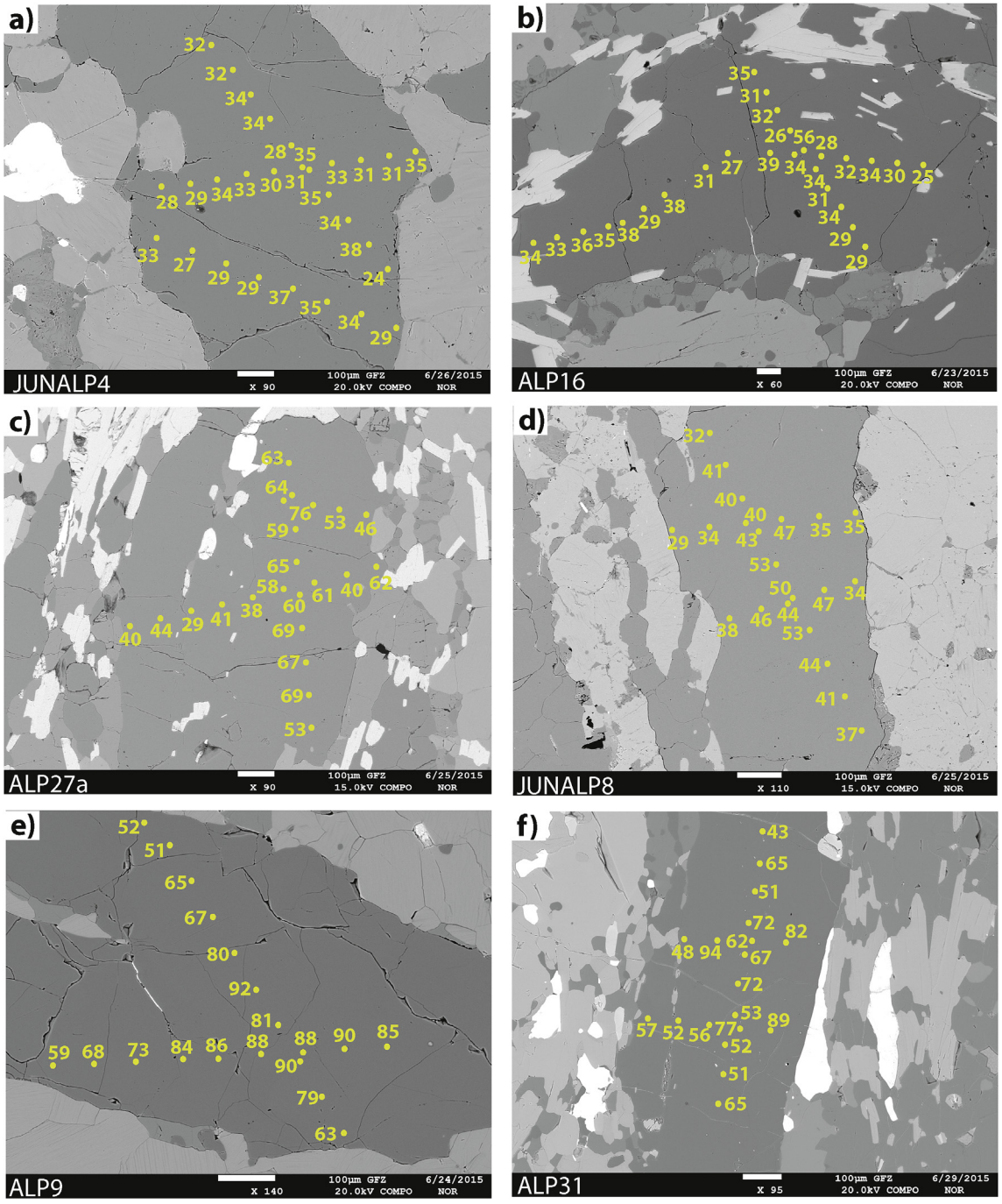

Fig. 11. Spots along transverse profiles and respective titanium concentrations (ppm) in quartz from the studied mylonitic rocks.

assumption of TitaniQ geothermometry that the Ti concentration primarily depends on the *P-T* conditions (e.g., Thomas et al., 2010, 2015). If equilibrium conditions were not reached during Huang and Audétat's experiments, and this led to variable values of Ti activity as suggested by Thomas et al. (2015), then it is possible that for the measured low Ti content and the assumed activities in our study (0.6–0.8), the highest temperature estimates > 740–822 °C obtained from the rocks from Além Paraíba and Sto. Antônio de Pádua, using the Huang and Audétat's calibration, may not be reliable. Under such temperatures and low pressure conditions (500–700 MPa; Porcher et al., 1995) quartzfeldsphatic rocks would probably melt (e.g., Bowen, 1956). However, no evidence of partial melting was observed in the studied rocks, and we therefore apply the Thomas et al. (2010) calibration and suggest that the maximum temperature in which quartz was deformed/recrystallized is ≤ 740 ± 20 °C.

The microstructures observed in all of our samples: irregular, smooth and lobate grain boundaries, large quartz ribbons, weak CPO, and indication of typically high-temperature slip systems, are consistent with the TitaniQ temperatures ranging from 612 to 740 °C, obtained using both calibrations, excluding the highest ones obtained from the Huang and Audétat calibration. Such a temperature range is also consistent with the temperatures obtained for mylonite development (615–785 °C) by Bento dos Santos et al. (2010) along the Além Paraíba-Pádua shear zone, and with mylonitization temperatures further north, in the Italva region (80 km NE of Sto Antônio de Pádua), where deformation seems to have occurred under 680–748 °C/650–700 MPa (e.g., Karniol et al., 2009). The highest temperatures (> 740–822 °C) however are more consistent with the ones obtained for metatexites

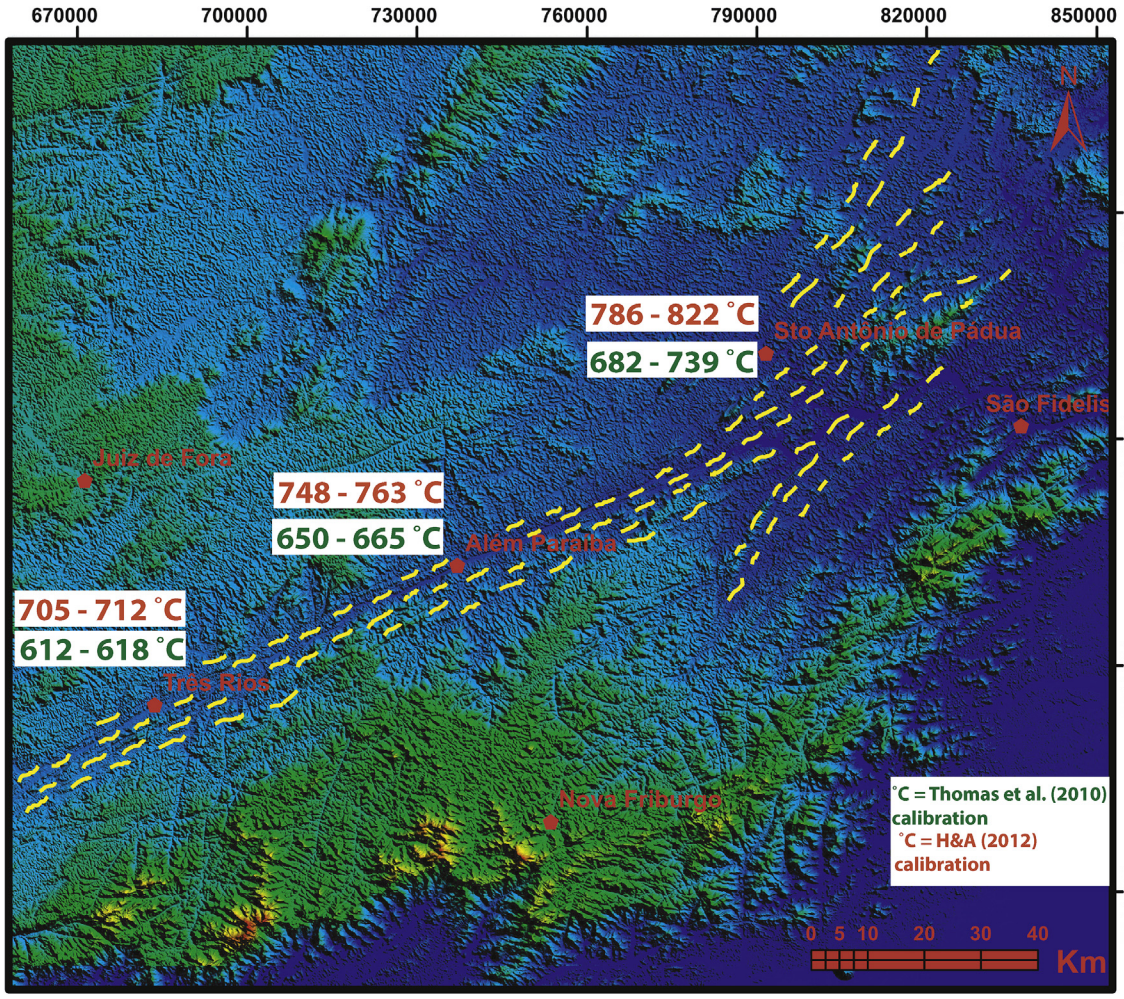

Fig. 12. Digital elevation model image displaying the TitaniQ average temperatures for mylonitic rocks from the Três Rios-Além Paraíba-Pádua shear zone (yellow lines mark shear zone boundaries). (For interpretation of the references to color in this figure legend, the reader is referred to the Web version of this article.)

(> 700–890 °C; Bento dos Santos et al., 2010), which once more suggest that under these higher temperatures, melt production would be efficient. Therefore, the highest temperatures obtained from Huang and Audetat's calibration are, at least in some regions, unreasonably high for the observed quartz recrystallization textures.

The rocks from the Três Rios-Além Paraíba-Sto Antônio de Pádua shear zone have evidence of expressive GBM recrystallization in quartz, and microstructures typical of high temperature conditions (≥550 °C), such as recrystallized feldspar grains (e.g., Vidal et al., 1980). In general, the temperatures obtained from both calibrations (612 - ≤ 740 °C) are consistent with the observed microstructures and quartz CPO, which suggest that TitaniQ geothermobarometer is a powerful tool to investigate temperature conditions during quartz deformation. However, as Huang and Audétat's calibration seems to overestimate temperature to a certain extent, care should be taken when choosing a single calibration to investigate temperature conditions during deformation. From this study and others (e.g., Cavalcante et al., 2014; Cross et al., 2015), one can suggest that both calibrations should be considered for temperature calculations, together with additional investigations such as microstructural and textural analysis.

10. Discussion

10.1. Microstructures, misorientation analysis and CPO data

The predominantly coarse-grained mylonites of the studied section of the Três Rios-Além Paraíba-Pádua shear zone consist of mineral phases that exhibit a diversity of microstructures (elongate enstatite and hornblende; feldspar with subgrains, undulose extinction, deformation twins, and core-and-mantle structure) characteristic of high-temperature deformation. Quartz grains from all the selected samples display abundant evidence of intracrystalline deformation, such as undulose extinction, ribbon shapes, and subgrain boundaries, as confirmed by the frequent low (~5°) misorientation angles (Fig. 9a–f). Irregular, smooth and lobate grain boundaries are common, especially in the quartz ribbons in which Ti content was measured. Quartz interfaces in the ribbons are often perpendicular to their long axes, and some quartz ribbons are large crystals with abnormally high aspect ratios (Figs. 4 and 6). These observations suggest that quartz deformation was accompanied by dynamic recrystallization by means of GBM with subsequent grain growth and SGR (e.g., Passchier and Trouw, 2005). The TitaniQ temperatures estimated in quartz ribbons (612- ≤740 °C) are quite high for the activation of SGR recrystallization (e.g., Stipp et al., 2002). Furthermore, Ti equilibration in quartz seems not to occur if deformation is only accompanied by SGR or BLG recrystallization, because the Ti volume diffusion is not efficient under low temperatures (< 500 °C; e.g. Grujic et al., 2011). On the other hand, under high temperatures (> 500 °C), GBM recrystallization promotes efficient Ti diffusion and consequently Ti reequilibration, i.e. if Ti content is reequilibrated under GBM conditions, subsequent SGR overprint does not reset this Ti content (e.g., Law, 2014). Therefore, the TitaniQ results obtained here likely record the deformation

temperatures in which quartz ribbons developed during GBM recrystallization.

Most samples show a prominent quartz misorientation angle maximum at 60° (Fig. 9), which mainly corresponds to the correlated misorientation distribution. This 60° maximum is consistent with Dauphiné twinning, as has been shown in several studies (e.g., Law et al., 1990; Lloyd, 2004; Menegon and Pennacchioni, 2010). It is also confirmed by the misorientation axis/angle pair, where the misorientation axes clustered close to the c-axis are those showing 60° misorientation angles (Fig. 9). Dauphiné twins are common in tectonites and are thought to have a mechanical weakening effect on quartz (e.g., Tullis, 1970).

The misorientation angles have distributions that do not deviate substantially from the random curve (uniform distribution) (Fig. 9), which suggests no or very weak crystallographic fabrics (e.g., Wheeler et al., 2001). The crystallographic fabrics defined by the pole figures are weaker than fabrics generally reported from high-temperature dislocation creep regimes (typically with c-axis close to the X-direction; Schmid et al., 1981; Stipp et al., 2002; Pennacchioni et al., 2010) (Fig. 8). The only exception is sample JUNALP8 (Fig. 8c) from the Além Paraíba region, which shows the strongest (but still weak) J-index value (3.6) and a single c-axis maximum close to X, suggesting the activation of prism < c > slip (e.g., Mainprice et al., 1986; Pennacchioni et al., 2010). Such a weak crystallographic fabric could be the result of high-temperature (612 to ≤ 740 °C) diffusive processes associated with GBM recrystallization and subsequent grain growth, or due to the occurrence of multiple slip systems (e.g., combined prism < c > + prism < a >, sample ALP16; prism < c > + rhomb < a >, sample JUNALP4). The interpretation of multiple slip systems is difficult based on the very weak crystallographic fabric, and the occurrence of slip in the < c +a > directions appears to be difficult in quartz (e.g., Linker et al., 1984). In fact, the misorientation axes for the misorientation angle interval 10–20° show multiple maxima, which might be an indication of multiple slip systems operating during the deformation of quartz grains. Apart from the suggestion of the prism < c > slip system depicted by the distribution of c-axis near the X-axis, a secondary concentration of poles close to Z-axis occur for the rhombohedral planes, notably for the positive rhombs in the pole figures, as well as in the distribution of misorientation axes for the crystal system.

A smooth morphology of quartz-quartz boundaries occurs within most ribbons (Figs. 5 and 6), and their orientation is perpendicular to the ribbons. This is expected if grain growth occurred during static recrystallization, i.e. after dynamic recrystallization (e.g., Culshaw and Fyson, 1984). Grain growth under static conditions usually does not result in the loss of previously formed CPO (e.g., Boullier and Bouchez, 1978), and can therefore not explain the weak fabrics, but may promote strain weakening (e.g., Heilbronner and Tullis, 2002).

Hippertt et al. (2001) show c-axis fabric diagrams with a clear maximum along or close to Z and suggest that basal < a > slip may have been the main operative glide in their samples. They interpreted the formation of quartz ribbons from the basal < a > glide activation at high temperatures (680–750 °C), due to deformation under dry conditions. In our samples, we do not observe any concentration of < c > axis along Z, and from the ribbons with the Dauphiné twinning the main slip system seems to be parallel to the < c > direction and one of the rhombohedral planes in the < a > direction.

Farther south in the Ribeira belt, Faleiros et al. (2016) show several patterns of c-axis CPO. For what they regard as high-T fabrics, they seem to get a maximum along Y, and locally also along X (their Fig. 11 a–d). In the high-pressure region of the Norwegian Caledonides (Western Gneiss Region), Renedo et al. (2015) found a concentration of quartz c-axes close the X-direction for eclogite deformed at 750–830 °C, which they interpret as evidence for prism < c > slip. Ribbon gneisses hosting the eclogite and deformed at somewhat lower temperatures have c-axis girdles perpendicular to the foliation, but with no marked concentration along Z. From the same region (but with poorly constrained temperatures between 800 and 600 °C), Barth et al. (2010) report generally weak fabrics and evidence for several different slip systems. A strong Y-maximum is reported from some other high-grade ribbon-bearing gneisses (McLelland, 1984; MacKinnon and Fueten, 1997), although the temperature in these cases are not well constrained.

In general, our data, in consistency with other published data sets, suggest that high (612 - ≤740 °C) temperature conditions can produce CPO patterns with a large variability in appearance. Even though prism < c > slip is strongly represented, high-temperature conditions seem to allow for activation of a wide range of competing slip systems that contribute to the variability of the generally weak microfabrics.

10.2. TitaniQ interpretation

Huang and Audétat (2012) calibration yielded temperatures ~ 80–100 °C higher than those calculated using the calibration of Thomas et al. (2010). Such higher temperatures have often been reported (e.g., Cavalcante et al., 2014; Ashley et al., 2013; Ashley and Law, 2015).

The average temperatures obtained using the calibration of Thomas et al. (2010) range from 612 °C in Três Rios region to 739 °C in Santo Antônio de Pádua region (Fig. 12). These temperature values can be considered as the maximum temperature for quartz recrystallization/deformation and agrees with the temperatures obtained in previous studies for mylonitization in the study area, within error of ± 20 °C (615–785 °C; Porcher et al., 1995; Bento dos Santos et al., 2010). Such temperatures are consistent with the activation of prism < c > slip in quartz (e.g., sample JUNALP8, Fig. 8c) and diffusive mechanisms capable of efficiently weakening the crystallographic fabric.

Our temperature estimates suggest that quartz from mylonitic rocks of the Três Rios-Além Paraíba-Pádua shear zone was deformed at temperatures below metamorphic peak (~800–890 °C; Porcher et al., 1995), under temperatures between 612 and ≤ 740 °C, and accompanied by dynamic recrystallization by GBM and subsequently SGR. Grujic et al. (2011) suggest that under high temperature deformation, Ti reequilibration is achieved mainly by GBM, and that GBM is crucial for the reequilibration of Ti-in-quartz. GBM therefore appears to be a very important recrystallization mechanism to promote diffusion in the crystal lattice along grain boundaries.

Our observed microstructures and mineral assemblage, together with misorientation angle patterns, suggest that dynamic recrystallization in the studied mylonites occurred under high-temperature conditions by GBM and SGR. SGR is expected to occur under temperatures > 400–500 °C, while GBM may occur at > 500 °C (e.g., Law, 2014; Stipp et al., 2002). Rocks deformed under amphibolite to granulite facies conditions in a transpressive shear zone may record microstructural evidence from multiple portions of the exhumation path. However, the quite consistent average values of Ti content between grains from the same sample and between samples from the same region suggest that Ti was equilibrated prior to exhumation-related cooling, and that early GBM recrystallization preserved the Ti content in the recrystallized quartz ribbons during the exhumation history (at high T). If the formation of subgrain boundaries occurred during later and cooler stages of exhumation, the SGR processes were probably not capable of resetting the Ti content equilibrated during GBM, as has been suggested in other studies (e.g., Grujic et al., 2011; Härtel et al., 2013; Kidder et al., 2013).

If temperature conditions during deformation were on the order of 740 °C for this segment of the shear zone, then the distance over which diffusional modification of the Ti-concentration in quartz could occur would be ~190 μm in a million years (estimated using the Arrhenius equation; Cherniak et al., 2007). This means that under such high temperature, just a few million years would suffice for efficient equilibration of the Ti content in quartz, even if quartz is coarse grained. However, if deformation occurred at 612 °C, then Ti diffusivity in quartz would occur over a distance of only ~18 μm in a million years,

while a distance of ~190 μm would require ~10 Myr. This implies that for the coarse quartz ribbons analyzed here (at least 500 μm in one of its directions), if the temperature for recrystallization was ~612 °C, the duration at which the rocks resided in the middle to lower crust should be much longer (≥27 Myr) than that expected for a temperature of ~740 °C (~2.6 Myr).

Bento do Santos et al. (2010), based on isotopic thermochronologic data from felsic granulites from the Além Paraiba-Pádua shear zone, concluded that these rocks were maintained at deep crustal levels under temperatures above 750 °C from ~570 Ma, maintaining temperatures in excess of 650 °C until 470–500 Ma (cooling rate of ~1 °C/Ma). These authors tentatively suggested that the unusually long residence period (~100 Myr) under such high temperatures was due to upwelling of asthenospheric mantle and magma underplating, coupled with long-term generation of high HPE (heat producing elements) granitoids along the main axis of the Ribeira Belt.

We do not know exactly for how long the rocks remained in the middle to lower crust under such high temperatures, only the minimum time intervals, which would be ~2.6 Myr at 740 °C and 27 Myr at 612 °C (based on the Arrhenius equation). However, even if we assume that temperatures during mylonitization reached ~612 °C in the Três Rios region, this implies that the whole studied shear segment resided at or close to this temperature for at least 27 Myr, consistent with previous thermochronologic data (Bento dos Santos et al., 2010, 2011). Such temperature conditions would also favor GBM as an important recrystallization mechanism for contributing to solid-state diffusion, and consequently, promoting grain growth and homogenization of the Ti distribution in the sample-scale from the same region, a weak crystallographic fabric in most samples, and activation of prism < c > slip system.

11. Concluding remarks

Addressing the applicability of TitaniQ geothermometer to high-temperature deformation in the Três Rios-Além Paraíba-Pádua transpressive shear zone, we measured the Ti content of large quartz ribbons that have similar microstructures and CPO fabrics. We found that maximum temperature conditions for quartz recrystallization is ≤740 °C if we apply Thoma's calibration. Although both calibrations provide temperatures that are consistent with the observed microstructures and CPO data, Huang and Audétat's calibration seems to overestimate the temperature to certain extent. Therefore, we believe that the most appropriate calibration for reconstructing the conditions of quartz recrystallization is the one by Thomas et al. (2010), as it takes into consideration the $aTiO_2$ and can be confidently applied to coarse-grained quartz. Temperatures from the Thomas et al. (2010) calibration are also consistent with independent geothermometric estimates, which suggest that mylonitization in the Além Paraíba-Pádua shear zone occurred under conditions ranging from 615 to 785 °C (Bento dos Santos et al., 2010).

The average Ti content from grains of the same sample and samples from the same region is fairly homogeneous, which requires an efficient mechanism and sufficiently high temperature conditions to promote homogenization of the Ti at the sample scale. GBM has often been suggested in previous studies as an effective mechanism to equilibrate Ti in quartz over short time scales (e.g., Grujic et al., 2011; Härtel et al., 2013; Kidder et al., 2013). Based on the quartz grain boundaries and the large grain sizes of our samples, we can infer that GBM was a major recrystallization mechanism during the mylonitization. Subgrains inside quartz ribbons suggest that quartz also recrystallized at temperatures below 612 °C, but SGR recrystallization was not efficient enough to modify the Ti content equilibrated during GBM, i.e. the Ti content equilibrated when temperature was between 612 and ≤ 740 °C. Smooth grain boundaries perpendicular to the long axis of the quartz ribbons indicate that Ti homogenization was also assisted by grain growth under static conditions, which may accentuate diffusion along the grain boundaries. Based on Ti diffusivity in quartz (Cherniak et al., 2007), we suggest that if temperature during deformation was ~612 °C, it would take at least 27 Myr for Ti to be equilibrated between quartz grains of the same sample. Such residence time is consistent with the thermal history proposed by Bento dos Santos et al. (2010), which suggests that the mylonitic rocks from the Além Paraíba-Pádua shear zone were maintained at temperatures between > 750 and > 650 °C for approximately 100 Myr.

The CPO fabric is weak, which indicates that diffusion processes may have operated during or right after dynamic recrystallization and dislocation creep. Prism < c > slip, typical for dislocation creep at high-temperatures, probably operated during shear zone development and contributed to initial strain softening and localization of deformation. However, other slip systems were also active, which helps explain the range in CPO patterns. Besides being favored by the high temperature conditions, strain softening was probably also favored by the quartz microstructure itself, and evidence of Dauphiné twinning is recorded in most samples.

In summary, our TitaniQ results and microstructural study suggest that deformation during the Três Rios-Além Paraíba-Pádua shear zone development occurred under temperatures ranging from 612 to ≤740 °C. The TitaniQ geothermometry and textural analysis together can be reliably applied to investigate temperature conditions during hot crystal-plastic deformation of mylonitic rocks extensively recrystallized by GBM.

Acknowledgments

This work was supported by Fundação de Amparo à Pesquisa do Estado de São Paulo (FAPESP) projects 2013/19061-0, 2014/10146-5, and 2015/23572/5. Jay B. Thomas is thanked for all his support on TitaniQ calculations, Fabrice Barou for his support during EBSD measurements, Oona Appelt for her very careful TitaniQ analysis, William Nachlas for his help with Arrhenius calculations, Pedro Augusto for his help during sampling, and William M. Dune and Enrique Gomez-Rivas for careful editorial handling of the submission. We are indebted to Richard Law and William Nachlas for constructive criticism and suggestions, which greatly improved our manuscript. Luiz Inácio Lula da Silva and Dilma Rousseff are thanked for promoting autonomy to science and the Brazilian people.

Appendix A. Supplementary data

Supplementary data related to this article can be found at https://doi.org/10.1016/j.jsg.2018.07.013.

References

Almqvist, B.S.G., Mainprice, D., 2017. Seismic properties and anisotropy of the continental crust: predictions based on mineral texture and rock microstructure. Rev. Geophys. 55, 367–433. https://doi.org/10.1002/2016RG000552.

Armstrong, J.T., 1995. CITZAF: a package of correction programs for the quantitative electron microbeam X-ray-analysis of thick polished materials, thin films, and particles. Microbeam Anal. 4, 177–200.

Ashley, K.T., Webb, L.E., Spear, F.S., Thomas, J.B., 2013. P–T–D histories from quartz: a case study of the application of the TitaniQ thermobarometer to progressive fabric development in metapelites. G-cubed 14 (9), 3821–3843.

Ashley, K.T., Law, R.D., 2015. Modeling prograde TiO2 activity and its significance for Ti-in-quartz thermobarometry of pelitic metamorphic rocks. Contrib. Mineral. Petrol. 169, 23. https://doi.org/10.1007/s00410-015-1118-7.

Barth, N.C., Hacker, B.R., Seward, G., Walsh, E.O., Young, D., Johnston, S., 2010. Strain within the ultrahigh-pressure western gneiss region of Norway recorded by quartz CPOs. In: In: Law, R.D., Butler, R.W.H., Holdsworth, R.E., Krabbendam, M., Strachan, R.A. (Eds.), Continental tectonics and Mountain Building: the Legacy of Peach and Horne, vol. 335. Geological Society, London, Special Publications, pp. 661–678.

Bento dos Santos, T.M., Munhá, J.M., Tassinari, C.C.G., Fonseca, P.E., Dias Neto, C., 2010. Thermochronology of central Ribeira Fold Belt, SE Brazil: petrological and geochronological evidence for long-term high temperature maintenance during Western Gondwana amalgamation. Precambrian Res. 180 (3–4), 285–298. https://doi.org/10.1016/j.precamres.2010.05.002.

Bento dos Santos, T., Munhá, J., Tassinari, C., Fonseca, P., Dias Neto, C., 2007. Thermochronological evidence for long-term elevated geothermal gradients in Ribeira Belt, SE Brazil. Geochem. Cosmochim. Acta 71 (15), A79 1.

Bento dos Santos, T.M., Munhá, J.M., Tassinari, C.C.G., Fonseca, P.E., Neto, C.D., 2011. Metamorphic P-T evolution of granulites in the central Ribeira fold belt, SE Brazil. Geosci. J. 15 (1), 27–51. https://doi.org/10.1007/s12303-011-0004-1.

Bento dos Santos, T., Fonseca, P., Munha, J., Tassinari, C., Dias Neto, C., 2009. Geodynamic evolution of the São Fidelis e Santo Antônio de Pádua sector, Ribeira Fold Belt, SE Brazil. Comun. Geol. 96, 101–122.
Bestmann, M., Pennacchioni, G., 2015. Ti distribution in quartz across a heterogeneous shear zone within a granodiorite: the effect of deformation mechanism and strain on Ti resetting. Lithos 227, 37–56.
Boullier, A.M., Bouchez, J.L., 1978. Le quartz en rubans dans les mylonites. Bull. Soc. Geol. Fr. 7, 253–262 Sdr. 20.
Bowen, N.L., 1956. The Evolution of the Igneous Rocks. Dover, Canada, pp. 60–62.
Brueckner, H.K., Cunningham, D., Alkmin, F.F., Marshak, S., 2000. Tectonic implications of Precambrian Sm–Nd dates from the southern São Francisco craton and adjacent Araçuaí and Ribeira belts, Brazil. Precambrian Res. 99, 255–269.
Bürgmann, R., Dresen, G., 2008. Rheology of the lower crust and upper mantle: evidence from rock mechanics, geodesy, and field observations. Annu. Rev. Earth Planet Sci. 36 (1), 531–567. https://doi.org/10.1146/annurev.earth.36.031207.124326.
Cavalcante, G.C.G., Vauchez, A., Merlet, C., Berzerra de Holanda, M.H., Boyer, B., 2014. Thermal conditions during deformation of partially molten crust from TitaniQ geothermometry: rheological implications for the anatectic domain of the Araçuaí belt, eastern Brazil. Solid Earth 5, 1223–1242. https://doi.org/10.5194/se-5-1223-2014.
Cherniak, D.J., Watson, E.B., Wark, D.A., 2007. Ti diffusion in quartz. Chem. Geol. 236 (1–2), 65–74. https://doi.org/10.1016/j.chemgeo.2006.09.001.
Cordani, U., Delhal, J., Ledent, D., 1973. Orogenéses superposées dans le Précambrien du Brésil sud-oriental (États de Rio de Janeiro et de Minas Gerais). Rev. Bras. Geociencias 3, 1–22.
Cross, A.J., Kidder, S., Prior, D.J., 2015. Using microstructures and TitaniQ thermobarometry of quartz sheared around garnet porphyroclasts to evaluate microstructural evolution and constrain an Alpine Fault Zone geotherm. J. Struct. Geol. 75, 17–31. https://doi.org/10.1016/j.jsg.2015.02.012.
Culshaw, N.G., Fyson, W.K., 1984. Quartz ribbons in high grade granite gneiss: modifications of dynamically formed quartz c-axis preferred orientation by oriented grain growth. J. Struct. Geol. 6, 663–668.
Faleiros, F.M., Campanha, G.A.C., Pavan, M., Almeida, V.V., Rodrigues, S.W.O., Araújo, B.P., 2016. Short-lived polyphase deformation during crustal thickening and exhumation of a collisional orogen (Ribeira Belt, Brazil). J. Struct. Geol. 93, 106–130. https://doi.org/10.1016/j.jsg.2016.10.006.
Ghent, E.D., Stout, M.Z., 1984. TiO_2 activity in metamorphosed pelitic and basic rocks: principles and applications to metamorphism in southeastern Canadian Cordillera. Contrib. Mineral. Petrol. 86, 248–255.
Grujic, D., Stipp, M., Wooden, J.L., 2011. Thermometry of quartz mylonites: importance of dynamic recrystallization on Ti-in-quartz reequilibration. G-cubed 12, Q06012. https://doi.org/10.1029/2010GC003368.
Härtel, M., Herwegh, M., Pettke, T., 2013. Titanium-in-quartz thermometry on synkinematic quartz veins in a retrograde crustal-scale normal fault zone. Tectonophysics 608, 468–481.
Heilbron, M., Ribeiro, A., Valeriano, C.M., Paciullo, F.V., Almeida, J.C.H., Trouw, R.J.A., Tupinambá, M., Eirado Silva, L.G., 2017. The Ribeira belt. In: Heilbron, M., Cordani, U., Alkmim, F.F. (Eds.), São Francisco Craton, Eastern Brazil. Springer, pp. 277–302. https://doi.org/10.1007/978-3-319-01715-0_1.
Heilbronner, R., Tullis, J., 2002. The effect of static annealing on microstructure and crystallographic preferred orientations of quartzites experimentally deformed in axial compression and shear. In: In: de Meer, S. (Ed.), Deformation Mechanisms, Rheology and Tectonics: Current Status and Future Perspectives, vol. 200. Geological Society London, Special Publications, pp. 191–218.
Hippertt, J., Rocha, A., Lana, C., Egydio-Silva, M., Takeshita, T., 2001. Quartz plastic segregation and ribbon development in high-grade striped gneisses. J. Struct. Geol. 23, 67–80.
Hirth, G., Tullis, J., 1992. Dislocation creep regimes in quartz aggregates. J. Struct. Geol. 14, 145–159.
Huang, R., Audétat, A., 2012. The titanium-in-quartz (TitaniQ) thermobarometer: a critical examination and re-calibration. Geochem. Cosmochim. Acta 84, 75–89. https://doi.org/10.1016/j.gca.2012.01.009.
Kidder, S., Avouac, J.P., Chan, Y.C., 2013. Application of titanium-in-quartz thermobarometry to greenschist facies veins and recrystallized quartzites in the Hsüehshan range, Taiwan. Solid Earth 4, 1–21 . https://doi.org/10.5194/se-4-1-2013.
Karniol, T.R., Machado, R., Bilal, E., Moutte, J., 2009. Geotermobarometria de granulitos do Cinturão Ribeira na porção norte do estado do Rio de Janeiro: seção Italva (RJ)-Patrocínio do Muriaé (MG). 39, 519–532.
Kohn, M.J., Northrup, C.J., 2009. Taking mylonite temperatures. Geology 37, 47–50. https://doi.org/10.1130/G25081A.1.
Lapworth, T., Wheeler, J., Prior, D.J., 2002. J. Struct. Geol. 24, 387–399.
Law, R.D., 2014. Deformation thermometry based on quartz < c > axis fabrics and recrystallization microstructures: a review. J. Struct. Geol. 66, 129–161 .
Law, R.D., Schmid, S.M., Wheeler, J., 1990. Simple shear deformation and quartz crystallographic fabrics: a possible natural example from the Torridon area of NW Scotland. J. Struct. Geol. 12, 29–45. https://doi.org/10.1016/j.jsg.2014.05.023.
Leloup, P.H., Kienast, J.R., 1993. High-temperature metamorphism in a major strike-slipshear zone: the Ailao Shan-Red River, People's Republic of China. Earth Planet Sci. Lett. 118, 213–234.
Linker, M.F., Kirby, S.H., Ord, A., Christie, J.M., 1984. Effects of compression direction on the plasticity and rheology of hydrolytically weakened synthetic quartz crystals at atmospheric-pressure. J. Geophys. Res. 89, 4241–4255.
Lloyd, G.E., Farmer, A., Mainprice, D., 1997. Misorientation analysis and the formation and orientation of subgrains and grain boundaries. Tectonophysics 279, 55–78.
Lloyd, G.E., 2004. Microstructural evolution in a mylonitic quartz simple shear zone: the significant roles of dauphine twinning and misorientation. In: In: Alsop, G.I., Holdsworth, R.E., McCaffrey, K., Hand, M. (Eds.), Transports and Flow Processes in Shear Zones, vol. 224. Geological Society London Special Publication, pp. 39–61.
Lowry, A.R., Pérez-Gussinyé, M., 2011. The role of crustal quartz in controlling Cordilleran deformation. Nature 471 (7338), 353–357. https://doi.org/10.1038/nature09912. .
Machado, R., 1984. Evolução geológica, análise estrutural e metamórfica da região de Vassouras e Paracambi, porção ocidental do Estado do Rio de Janeiro. Instituto de Geociências, Universidade de São Paulo, São Paulo, Tese de Doutoramento, pp. 196.
Machado, N., Valladares, C., Heilbron, M., Valeriano, C., 1996. U-Pb geochronology of the central Ribeira belt (Brazil) and implications for the evolution of the Brazilian orogeny. Precambrian Res. 79, 347–361.
MacKinnon, P., Fueten, F., 1997. A fracture model for quartz ribbons in straight gneisses. J. Struct. Geol. 19, 1–14.
Mainprice, D., Bouchez, J.L., Blumenfeld, P., Tubia, J.M., 1986. Dominant c-slip in naturally deformed quartz: implications for dramatic plastic softening at high temperature. Geology 14, 819–822.
McLelland, J.M., 1984. The origin of ribbon lineation within the southern Adirondacks. U.S.A. J. Struct. Geol. 6, 147–157.
Menegon, L., Pennacchioni, G., 2010. Local shear zone pattern and bulk deformation in the Gran Paradiso metagranite (NW Italian Alps). Int. J. Earth Sci. 99 (8), 1805–1825. https://doi.org/10.1007/s00531-009-0485-6.
Menegon, L., Nasipuri, P., Stünitz, H., Behrens, H., Ravna, E., 2011. Dry and strong quartz during deformation of the lower crust in the presence of melt. J. Geophys. Res. Solid Earth (B10), 116 1978-2012.
Nachlas, W.O., Whitney, D.L., Teyssier, C., Bagley, B., Mulch, A., 2014. Titanium concentration in quartz as a record of multiple deformation mechanisms in an extensional shear zone. G-cubed 15 (4), 1374–1397.
Nachlas, W.O., Hirth, G., 2015. Experimental constraints on the role of dynamic recrystallization on resetting the Ti-in-quartz thermobarometer. J. Geophys. Res.: Solid Earth 120, 8120–8137.
Negrini, M., Stünitz, H., Berger, A., Morales, L.F.G., 2014. The effect of deformation on the TitaniQ geothermometer: an experimental study. Contrib. Mineral. Petrol. 167, 982. https://doi.org/10.1007/s00410-014-0982-x.
Passchier, C.W., Trouw, R.A.J., 2005. Microtectonics, second ed. Springer, Berlin.
Pennacchioni, G., Menegon, L., Leiss, B., Nestola, F., Bromiley, G., 2010. Development of crystallographic preferred orientation and microstructure during plastic deformation of natural coarse-grained quartz veins. J. Geophys. Res. 115 (B12405), 23. https://doi.org/10.1029/2010JB007674.
Porcher, C., Egydio-Silva, Fernandes L., Vauchez, M., Dados, A., 1995. Preliminares do metamorfismo M1 da Faixa Ribeira: Região de Três Rios e Santo Antônio de Pádua (RJ). In: V Simpósio Nacional de Estudos Tectônicos, Gramado, Brasil, 1995, pp. 71–73 .
Renedo, R.N., Nachlas, W.O., Whitney, D.L., Teyssier, C., Piazolo, S., Gordon, S.M., Fossen, H., 2015. Fabric development during exhumation from ultrahigh-pressure in an eclogite-bearing shear zone, Western Gneiss Region, Norway. J. Struct. Geol. 71, 58–70. https://doi.org/10.1016/j.jsg.2014.09.012.
Schmid, S., Casey, M., Starkey, J., 1981. An illustration of the advantages of a complete texture analysis described by the orientation distribution function (ODF) using quartz pole figure data. Tectonophysics 78, 101–117.
Schmitt, R. d. S., Trouw, R., Van Schmus, W.R., Pimentel, M., 2004. Late amalgamation in the central part of Western Gondwana: new geochronological data and the characterization of a Cambrian collision orogeny in the Ribeira Belt (SE Brazil). Precambrian Res. 133, 29–61.
Schmitt, R. d. S., Trouw, R., Van Schmus, W.R., Armstrong, R., Stanton, N.S.G., 2016. The tectonic significance of the Cabo Frio Tectonic Domain in the SE Brazilian margin: a Paleoproterozoic through Cretaceous saga of a reworked continental margin. Braz. J. Geol. 46, 37–66. https://doi.org/10.1590/2317-4889201620150025.
Stipp, M., Stünitz, H., Heilbronner, R., Schmid, D.W., 2002. The eastern Tonale fault zone: a natural laboratory for crystal plastic deformation of quartz over a temperature range from 250 to 700 °C. J. Struct. Geol. 24, 1861–1884.
Thomas, J.B., Watson, E.B., Spear, F.S., Shemella, P.T., Nayak, S.K., Lanzirotti, A., 2010. TitaniQ under pressure: the effect of pressure and temperature on the solubility of Ti in quartz. Contrib. Mineral. Petrol. 160, 743e759.
Thomas, J.B., Watson, E.B., Spear, F.S., Wark, D.A., 2015. TitaniQ recrystallized: experimental confirmation of the original Ti-in-quartz calibrations. Contrib. Mineral. Petrol. 169 (27), 1–16.
Trouw, R., Heilbron, M., Ribeiro, A., Paciullo, F., Valeriano, C., Almeida, J., Tupinambá, M., Andreis, R., 2000. The central segment of the Ribeira Belt. In: Cordani, U.G., Milani, E.J., Thomaz-Filho, A., Campos, D.A. (Eds.), Tectonic Evolution of South America, pp. 297–310 Rio de Janeiro.
Trouw, R.A.J., Passchier, C.W., Wiersma, D.J., 2010. Atlas of Mylonites and Related Microstructures. Springer.
Tullis, J., 1970. Quartz — preferred orientations in rocks produced by Dauphiné twinning. Science 168 (3937), 1342–1344 .
Vauchez, A., Tommasi, A., Egydio-Silva, M., 1994. Self-indentation of a heterogeneous continental lithosphere. Geology 22, 967–970.
Vidal, J.L., Kubin, L., Debat, P., Soula, J.C., 1980. Deformation and dynamic recrystallization of K feldspar augen in orthogneiss from Montagne Noire, Occitania, Southern France. Lithos 13, 247–255 0024-4937.
Wark, D.A., Watson, E.B., 2006. TitaniQ: a titanium-in-quartz geothermometer. Contrib. Mineral. Petrol. 152, 743–754. https://doi.org/10.1007/s00410-006-0132-1.
Wheeler, J., Prior, D.J., Jiang, Z., Spiess, R., Trimby, P.J., 2001. The petrological significance of misorientations between grains. Contrib. Mineral. Petrol. 141, 109–124.